

ESTIMATING STAR FORMATION RATES FROM INFRARED AND RADIO LUMINOSITIES: THE ORIGIN OF THE RADIO–INFRARED CORRELATION

ERIC F. BELL¹

Steward Observatory, University of Arizona, 933 North Cherry Avenue, Tucson, AZ 85721, USA

THE ASTROPHYSICAL JOURNAL: *accepted on December 5th, 2002*

ABSTRACT

I have assembled a diverse sample of galaxies from the literature with far-ultraviolet (FUV), optical, infrared (IR) and radio luminosities to explore the calibration of radio-derived and IR-derived star formation (SF) rates, and the origin of the radio-IR correlation. By comparing the 8–1000 μ m IR, which samples dust-reprocessed starlight, with direct stellar FUV emission, I show that the IR traces most of the SF in luminous $\sim L_*$ galaxies but traces only a small fraction of the SF in faint $\sim 0.01L_*$ galaxies. If radio emission were a perfect SF rate indicator, this effect would cause easily detectable curvature in the radio-IR correlation. Yet, the radio-IR correlation is nearly linear. This implies that the radio flux from low-luminosity galaxies is substantially suppressed, compared to brighter galaxies. This is naturally interpreted in terms of a decreasing efficiency of non-thermal radio emission in faint galaxies. Thus, the linearity of the radio–IR correlation is a conspiracy: both indicators underestimate the SF rate at low luminosities. SF rate calibrations which take into account this effect are presented, along with estimates of the random and systematic error associated with their use.

Subject headings: radio continuum: galaxies — infrared: galaxies — ultraviolet: galaxies — dust, extinction — galaxies: general — cosmic rays

1. INTRODUCTION

Because ultraviolet (UV) and optical star formation (SF) rate indicators are so sensitive to dust (see, e.g., Kennicutt 1998; Adelberger & Steidel 2000; Bell & Kennicutt 2001; Goldader et al. 2002; Bell 2002), there has been much recent interest in using infrared (IR) and radio luminosities in their stead (see, e.g., Blain et al. 1999; Flores et al. 1999; Haarsma et al. 2000; Hopkins et al. 2001; Mann et al. 2002). While IR emission is straightforward to understand in the optically-thick case for an intensely star-forming galaxy (Kennicutt 1998), radio emission is a highly indirect indicator of SF rate, relying largely on the complex and poorly-understood physics of cosmic ray generation and confinement (see the excellent review by Condon 1992). Indeed, the strongest argument for radio luminosity as a SF rate indicator has come from the astonishingly tight (a factor of two over 5 orders of magnitude in luminosity) and arguably linear radio-IR correlation (e.g., de Jong et al. 1985; Condon et al. 1991; Yun et al. 2001). This close link between the radio and IR luminosities of galaxies, even when normalized by galaxy mass (e.g., Fitt et al. 1988; Price & Duric 1992), has often been used as a supporting argument for the efficacy and robustness of radio- and IR-derived SF rates. In this paper, I compare UV, H α , IR and radio luminosities for a diverse sample of galaxies to demonstrate that neither the IR nor radio emissions linearly track SF rate. I argue that the tight, nearly linear radio-IR correlation is a conspiracy: both the IR and radio luminosities of dwarf galaxies significantly underestimate the SF rate. Finally, new SF rate calibrations which take into account this effect are presented.

1.1. *The origin of IR and radio emission*

The primary prerequisite for an effective SF rate indicator is that it reflects the mass of young stars in some well-defined way. However, in practice, no SF rate indicator directly reflects the mass of young stars. It is useful at this stage to develop an

intuition for the physical origin, strengths and limitations of IR and radio emissions as SF rate indicators. For more in-depth discussion of these SF rate indicators, see Kennicutt (1998) and Condon (1992).

1.1.1. *IR emission*

In systems with ongoing SF, the light from both newly-formed and older stars can be absorbed by dust and reprocessed into the IR. There are thus two questions that should be addressed. *i)* What are the relative contributions of old and young stars to the IR luminosity? *ii)* How much light is reprocessed into the IR? Put differently, what is the optical depth of galaxies? Because of my focus on the young stellar populations, I will tend to focus on the optical depth of galaxies to light from young stars.

The relative balance of dust heating by young and old stars in star-forming galaxies is a matter of some debate. One observational indicator of this balance is the temperature of the dust. Young stars in H II regions heat up dust to relatively high temperatures (with a low 100 μ m to 60 μ m ratio of ~ 1). Older stars in the field, and far-ultraviolet (FUV) light from field OB associations (which have dispersed their natal clouds and so are relatively unattenuated in the FUV), heat the dust to much lower temperatures (100/60 $\gtrsim 5$; see, e.g., Lonsdale Persson & Helou 1987; Buat & Xu 1996; Walterbos & Greenawalt 1996). This difference between H II region and diffuse dust temperatures leads to a wide range in 100 μ m/60 μ m on galaxy-wide scales, from ~ 10 for quiescent early-type spiral galaxies through to $\lesssim 1$ for the most intensely star-forming galaxies. This suggests that earlier types are influenced more by old stellar populations than later types; this is also supported by an analysis of far-IR (FIR) and H α data by Sauvage & Thuan (1992). For a ‘median’ spiral galaxy, the ‘cold’ dust IR luminosity fraction is between 50% and 70% (Lonsdale Persson & Helou 1987; Bothun, Lonsdale & Rice 1989). Despite this domination by cooler dust, more recently it has been argued that the young, FUV-bright stars provide the dominant contribution to the IR flux ($\sim 70\%$; see, e.g., Buat & Xu 1996; Popescu et al. 2000; Misiriotis et al.

¹Present address: Max Planck Institut für Astronomie, Königstuhl 17, D-69117 Heidelberg, Germany; bell@mpia.de

2001). This is because FUV light is absorbed much more efficiently than optical light per unit dust mass. Thus, for a ‘median’ spiral galaxy, the IR luminosity comes from three components in roughly equal amounts: $\sim 1/3$ of the IR is from warm dust heated by FUV light from intense SF in H II regions, another $\sim 1/3$ is cold dust heated by optical photons from the old and young stellar populations, and the last $\sim 1/3$ of the IR is from cold dust heated by FUV light from OB associations in the field (Buat & Xu 1996). This interesting issue is discussed further in §4.

Given the apparent dominance of young stars in determining the IR flux, it is appropriate to address the opacity of dust to light from young stars. Observationally, there is a strong but scattered correlation between galaxy luminosity (\sim mass) and dust opacity to UV or H α light (Wang & Heckman 1996; Adelberger & Steidel 2000; Bell & Kennicutt 2001; Hopkins et al. 2001; Sullivan et al. 2001; Buat et al. 2002). Low-luminosity galaxies ($L/L_* \sim 1/100$) tend to have substantially less dust absorption and reddening than high-luminosity galaxies ($\sim L_*$). Furthermore, these papers demonstrate that low-luminosity galaxies have $IR/FUV \lesssim 1$, meaning that the IR emission of low-luminosity galaxies misses most of the SF. In contrast, many high-luminosity galaxies have $IR/FUV \gg 1$, implying that the IR may be a relatively good SF rate indicator in this case (Wang & Heckman 1996; Buat et al. 2002, §2.4). This will have clear implications for IR-derived SF rates, and correlations involving IR luminosities, such as the radio–IR correlation. This paper explores these implications in detail.

1.1.2. Radio emission

Radio continuum emission from star-forming galaxies has two components: thermal bremsstrahlung from ionized Hydrogen in H II regions (see, e.g., Caplan & Deharveng 1986), and non-thermal synchrotron emission from cosmic ray electrons spiraling in the magnetic field of the galaxy (see, e.g., Condon 1992, for an excellent review). Thermal radio emission has a spectrum $\propto \nu^{-0.1}$, whereas non-thermal emission has a much steeper radio spectrum $\propto \nu^\alpha$, where $\alpha \sim -0.8$ (however, note that α can vary, and even can vary with frequency; Condon 1992). Because of this difference in spectral shape, the relative contributions of the two emissions vary with frequency. At lower frequencies $\lesssim 5$ GHz non-thermal radiation tends to dominate (at 1.4 GHz, the ‘standard model’ of star-forming galaxies attributes typically 90% of the radio continuum flux of luminous spiral galaxies to non-thermal emission; Condon 1992). Based on the standard model, thermal emission may dominate at frequencies $\gtrsim 10$ GHz (see also Price & Duric 1992). In addition, the relative fractions of thermal and non-thermal emission may depend on galaxy mass. Dwarf galaxies seem to have a lower non-thermal to thermal emission ratio than normal spiral galaxies (Klein, Wielebinski & Thuan 1984; Klein 1991; Klein et al. 1991; Price & Duric 1992), although estimating the balance of thermal and non-thermal radio emission is painfully difficult, and can be uncertain for even well-studied galaxies at a factor of five level (Condon 1992). This difference between dwarf and larger galaxies is often interpreted as a higher efficiency of cosmic ray confinement in physically larger (or more massive) galaxies (e.g., Klein, Wielebinski & Thuan 1984; Chi & Wolfendale 1990; Price & Duric 1992). For interesting discussions about the relative balance of non-thermal and thermal emission see Condon (1992) and Niklas et al. (1997).

1.2. The Radio–IR correlation

Given the complexity of the emission mechanisms of radio continuum and IR light, it seems to be a miracle that the two fluxes are tightly correlated, with a scatter of only a factor of two. Yet, when examined closely, the radio–IR correlation betrays the richness of the astrophysics which determine galaxies’ radio and IR luminosities.

The slope of the radio–IR correlation seems to depend on galaxy luminosity. Samples which are richer in relatively faint galaxies ($L_{IR} \lesssim 10^{10} L_\odot$) tend to have steep radio–IR correlations in the sense that $L_{radio} \propto L_{IR}^\gamma$ and $\gamma > 1$ (e.g., Cox et al. 1988; Price & Duric 1992; Xu et al. 1994), whereas samples with a better representation of highly luminous galaxies ($10^{10} L_\odot \lesssim L_{IR} \lesssim 10^{12.5} L_\odot$) tend to have slopes close to unity (e.g., Condon et al. 1991; Yun et al. 2001). The differing behavior of galaxies as a function of luminosity is beautifully illustrated in Fig. 5 of Yun et al. (2001) and Figs. 1 and 2 of Condon et al. (1991). In addition, the slope depends on the radio frequency. At low radio frequencies $\lesssim 5$ GHz the slope tends to be steeper than unity, whereas for higher frequencies the slope approaches unity (wonderfully illustrated in Fig. 2 of Price & Duric 1992).

Workers in this field have typically sought to explain the luminosity-dependent slope in terms of heating of dust by older stellar populations, or non-thermal/thermal radio effects. Fitt et al. (1988) and Devereux & Eales (1989) both subtracted off plausible contributions from old stellar populations (using either FIR color θ or total IR luminosity as the constraint), which they found ‘linearized’ the radio–IR correlation. Condon et al. (1991) compared IR/radio with optical B /radio, finding that IR-overluminous galaxies were overluminous in optical B -band ($\sim 4400\text{\AA}$), which was interpreted as indicating contributions from old stellar populations. Xu et al. (1994) presented a model which described the non-unity slope and some of the scatter of the radio–IR correlation in terms of the contributions of old stellar populations. Similarly, a number of studies have investigated the rôle of non-thermal/thermal emission on the radio–IR correlation. Price & Duric (1992) and Niklas (1997) find that thermal radio continuum (which directly reflects the SF rate) correlated linearly with the IR luminosity; however, non-thermal emission had a steeper correlation with IR luminosity with $\gamma \sim 1.3$. Taken together, the steepening of the radio–IR correlation at low IR luminosities, and with decreasing radio frequency, have been interpreted as reflecting increasingly large contributions from old stellar population heating of the IR towards low IR luminosities, and non-thermal radio emission which is non-linearly related to the SF rate.

1.3. The goal of this paper

In contrast with the commonly accepted picture, I argue that these interpretations of the radio–IR correlation are incomplete because they neglect the effect of dust opacity on the IR emission of star-forming galaxies (note that Lisenfeld et al. 1996, briefly discussed the role of dust opacity, but not in a luminosity-dependent sense). The argument can be (but has not been, as yet) pieced together from results in the literature. Empirically, high-luminosity galaxies are optically thick to FUV light, and so their IR emission reflects the SF rate reasonably well. In contrast, low-luminosity galaxies have low IR/FUV; therefore, their IR emission underestimates the SF rate substantially (Wang & Heckman 1996). Yet the radio–IR correlation is more or less linear (e.g., Yun et al. 2001). Therefore, the radio

emission must be suppressed for low-luminosity galaxies. This offers independent support to the argument that low-luminosity galaxies tend to have substantially suppressed non-thermal radio emission (e.g., Klein, Wielebinski & Thuan 1984; Klein 1991; Price & Duric 1992). Thus, the radio–IR correlation is linear not because both emissions reflect SF rate perfectly, but because both radio and IR emissions underestimate the SF rates of low-luminosity galaxies in coincidentally quite similar ways.

In this paper, I assemble a sample of star-forming galaxies with FUV, IR and radio data to quantitatively explore this basic argument for the first time. The result that low-luminosity galaxies have IR and radio emissions that underestimate their SF rates is not new (e.g., Wang & Heckman 1996; Klein, Wielebinski & Thuan 1984; Dale et al. 2001). However, the assembly of an extensive star-forming galaxy sample with FUV, IR and radio data, the quantitative exploration of the consequences of this result on the radio–IR correlation, and the presentation of SF rate calibrations which take into account this effect, are new.

The plan of this paper is as follows. I first investigate, in detail, dust opacity indicators, and trends in dust opacity with galaxy luminosity, in §2. The galaxy sample is also introduced there. In §3, the radio–IR correlation is constructed, and the effect of dust opacity on the radio–IR correlation is estimated. In §4, the effect of optical light from old stellar populations is discussed. In §5, deviations from the expected trends in the radio–IR correlation are used to investigate the relationship between radio emission and SF rate. In §6, new IR and radio SF rate calibrations are presented and discussed. In §7, I summarize the conclusions of this study. In Appendix A, the FUV, optical, IR and radio data are discussed in more detail, and I present a table of galaxy photometry. In Appendix B, I present and discuss in detail a model for a luminosity-dependent FUV optical depth. Sections 2.1–2.3, §4, and the appendices are less central to my discussion of IR/radio SF rates, and may be skipped by casual readers. A distance scale compatible with $H_0 = 75 \text{ km s}^{-1} \text{ Mpc}^{-1}$ is assumed, and unless stated otherwise, I correct FUV and optical data for galactic foreground extinction using Schlegel et al. (1998).

2. UNDERSTANDING DUST OPACITY IN THE LOCAL UNIVERSE

In order to understand the implications of a correlation between dust opacity and luminosity, it is important to understand both the overall amount of opacity and the increase in the amount of opacity with luminosity in the wavelength regions that contribute the most to the heating of dust. Radiative transfer modeling coupled with observations (e.g., Buat & Xu 1996; Gordon et al. 2000) suggest that the bulk of the energy that goes into heating the dust comes from non-ionizing FUV light, between 1216\AA and $\sim 3000\text{\AA}$. Clearly, then, the vital question that must be addressed is that of the optical depth of dust to FUV light in a wide range of galactic environments.

2.1. Estimating the FUV optical depth of galaxies

There are three established methods for estimating the FUV attenuation² in star-forming galaxies.

- UV spectral slopes were found to correlate strongly with optical and FUV extinction, as estimated using

²Attenuation differs from extinction in that attenuation describes the amount of light lost because of dust at a given wavelength in systems with complex star/dust geometries where many classic methods for determining extinction, such as color excesses, may not apply.

a variety of observational techniques, for *starburst galaxies* (Calzetti et al. 1994, 1995; Meurer, Heckman, & Calzetti 1999). Because of its observational efficiency, this method has been extensively utilized at high redshift (see, e.g., Adelberger & Steidel 2000, and references therein). However, it has recently been shown that UV spectral slopes are poor attenuation indicators for other types of galaxy (Bell 2002; Goldader et al. 2002). Thus, I will not use this indicator in this paper.

- Total H I and/or H₂ column density has been used to estimate dust content, and therefore FUV extinction (e.g., Buat, Deharveng & Donas 1989). However, a number of factors, such as metallicity (through the dust-to-gas ratio), dust/star geometry, or extinction curve will introduce considerable scatter into any correlation between gas density and extinction. This was confirmed by Buat (1992) and Xu et al. (1997). Thus, I will not use gas density-derived extinctions in this paper.
- The TIR/FUV ratio, where TIR is the total 8–1000 μm luminosity and $F_{\text{FUV}} = \lambda F_{\lambda} = \nu F_{\nu}$ at $\sim 1550\text{\AA}$ (in this particular case) is, in principle, an excellent indicator of the amount of FUV extinction. This indicator of the direct vs. obscured light from young stars is a robust estimator of the FUV attenuation A_{FUV} , and is relatively unaffected by changes in dust extinction curve, star/dust geometry and SF history (Gordon et al. 2000). The main limitations of this method are *i*) that the rôle of older stellar populations in heating the dust is neglected (although it can be accounted for by using a more realistic method to estimate A_{FUV} , such as the flux-ratio method; Gordon et al. 2000), and *ii*) that some asymmetric star/dust geometries affect TIR/FUV (e.g., for a system with a dust torus, TIR/FUV would overestimate the FUV extinction and total SF rate if viewed pole-on, and would underestimate the total SF rate if viewed edge-on). Despite its limitations, I will use this method in this paper, not least because a greater understanding of the IR emission is one of the central goals of this work. This attenuation indicator has been used extensively before by, e.g., Buat (1992), Adelberger & Steidel (2000), Buat et al. (2002), and Bell (2002), and is directly related to the IR excess of Meurer, Heckman, & Calzetti (1999).

2.2. The Sample

Because of my focus on exploring the rôle of dust opacity and its effects on the radio–IR correlation, I have selected a sample of 249 galaxies that for the most part have *both* FUV and IR luminosities in the literature. The sample properties, a more in-depth discussion of the systematic and random errors, and a table of the relevant data is presented in Appendix A. Here, I briefly discuss only the most important points.

Normal, star-forming spiral and irregular galaxies were taken from Rifatto, Longo & Capaccioli (1995b, 100 galaxies), the *Far Ultraviolet Space Telescope* (FAUST; Deharveng et al. 1994, 75 galaxies) and the *Ultraviolet Imaging Telescope* (UIT; Bell & Kennicutt 2001, 37 galaxies). FUV flux uncertainties from Rifatto, Longo & Capaccioli (1995b) may be as large as

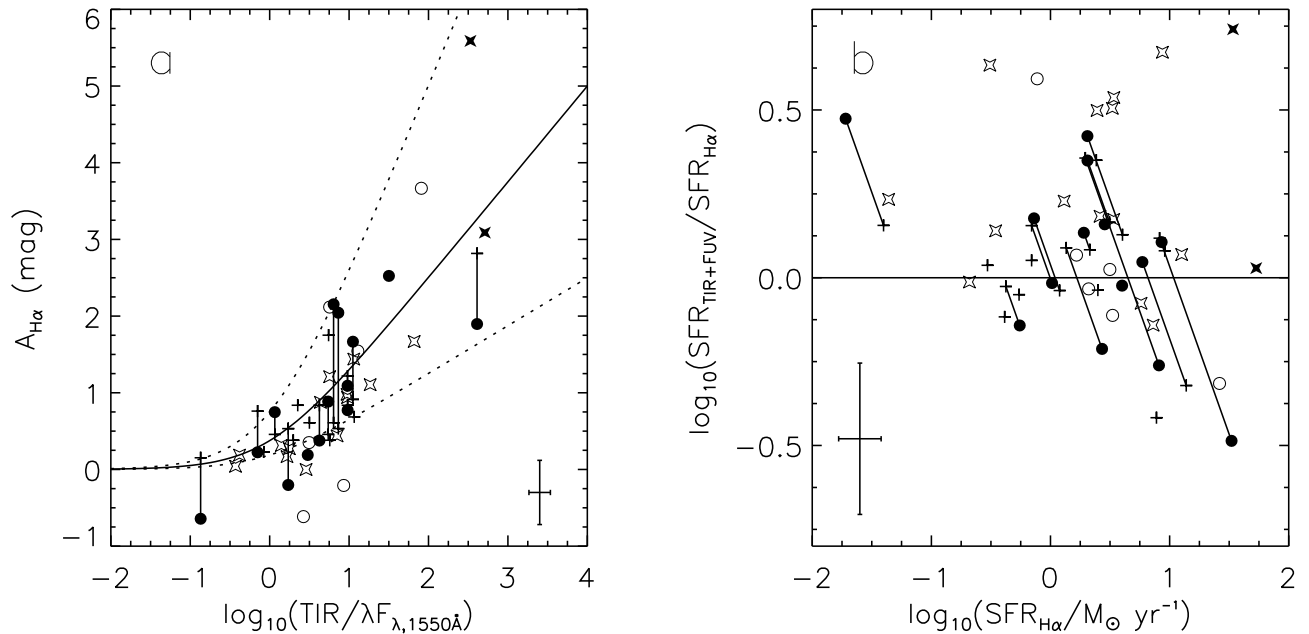


FIG. 1.— Intercomparison of attenuation in the FUV and at $H\alpha$. Panel *a*) shows the $H\alpha$ attenuation $A_{H\alpha}$ against TIR/FUV. Circles denote normal galaxies with (uncertain) thermal radio-derived $H\alpha$ attenuations (filled circles are UIT and FAUST galaxies, open circles are from Rifatto, Longo & Capaccioli 1995b). Crosses denote normal galaxies with Balmer-derived $H\alpha$ attenuations. Open stars denote starbursting galaxies and filled stars denote ULIRGs (both have Balmer-derived $H\alpha$ attenuations). The solid line is the relationship between the two that would be expected if TIR/FUV were a perfect indicator of FUV attenuation, and assuming that the $H\alpha$ attenuation is 1/2 of the FUV attenuation. The dotted lines show the relationship if the $H\alpha$ were 1/4 of, or the same as, the FUV attenuation. Panel *b*) shows the ratio of the TIR+FUV SF rate and the $H\alpha$ -derived SF rate, against the $H\alpha$ -derived SF rate. The symbols are the same as in panel *a*). The solid line denotes equality. In both panels the typical errors are shown, and thermal/Balmer measurements for the same galaxy are connected.

0.19 dex (larger galaxies, with substantially larger uncertainties, were removed from this sample). Flux uncertainties for galaxies from Deharveng et al. (1994) and Bell & Kennicutt (2001) are lower, ~ 0.08 dex. Intensely star-forming galaxies have also been added to the sample. Starbursting galaxies (Calzetti et al. 1994, 1995, 22 galaxies) have $10'' \times 20''$ FUV fluxes from the *International Ultraviolet Explorer* (IUE). To limit the effects of aperture bias, I use only the FUV data for the 14 starburst galaxies with optical diameters $\leq 1.5'$. Eight larger starbursts are included in this study, but are assumed to have no FUV data (i.e. only the optical, IR and radio data are used). The typical measurement accuracy of the FUV fluxes is $\lesssim 0.08$ dex; clearly, the systematic aperture bias is more of a concern. Seven ultra-luminous infrared galaxies (ULIRGs) (Goldader et al. 2002) were added to the sample, with a typical FUV accuracy of $\lesssim 0.12$ dex. Eight Blue Compact Dwarves (BCDs) have been added to the sample also to check for consistency with other galaxy types (Hopkins et al. 2002). FUV fluxes are quoted at wavelengths within 100\AA of 1550\AA : the error introduced by assuming that they are all at 1550\AA is $\sim 6\%$. In the remainder of this paper, these $\sim 1550\text{\AA}$ fluxes are denoted as ‘FUV’ fluxes or ‘ 1550\AA ’ fluxes. Note also that galaxies classified as Seyferts in the NASA/IPAC Extragalactic Database have been removed from the sample.

IR data at $12\text{--}100\mu\text{m}$ was taken from the *Infrared Astronomical Satellite* (IRAS) for 245 galaxies, and is accurate to better than 20% in both a random and systematic sense (Rice et al. 1988; Soifer et al. 1989; Moshir et al. 1990; Tuffs et al. 2002). Total IR $8\text{--}1000\mu\text{m}$ (TIR) and $42.5\text{--}122.5\mu\text{m}$ (FIR) fluxes were derived from the IRAS data, and are accurate to $\sim 30\%$ (see the

discussion in Appendix A). In this paper, I adopt the TIR $8\text{--}1000\mu\text{m}$ fluxes, in order to more accurately probe the true relationship between the amount of light reprocessed by dust into the IR with the radio emission (e.g., Dale et al. 2001, find a ‘normal’ FIR-to-radio ratio for the starbursting SBS 0335–052 but a large TIR-to-radio ratio because of a large population of hot dust). The $42.5\text{--}122.5\mu\text{m}$ FIR fluxes are only used as a consistency check; all the results in this paper apply to both TIR and FIR fluxes, taking into account that $\text{FIR} \sim 0.5 \text{ TIR}$ (see Appendix A for more details).

Optical data were carefully taken from the literature, using the NASA/IPAC Extragalactic Database and NASA’s Astrophysics Data System. Optical data for 247 galaxies was taken from a variety of sources and is accurate to $\lesssim 0.2$ mag in most cases, and to $\lesssim 0.5$ mag in all cases. Radio data for 166 galaxies at 1.4 GHz were, for the most part, taken from the NRAO VLA Sky Survey (NVSS; Condon et al. 1998). NVSS data were taken for 159 galaxies from Condon et al. (2002), Hopkins et al. (2002), and Gavazzi & Boselli (1999a,b) in that order of preference. Additional data at frequencies between 1.4 and 1.5 GHz (translated to 1.4 GHz assuming a $\nu^{-0.8}$ non-thermal spectrum) were taken from other sources for seven galaxies which were not in the above catalogs, but were important to have in the sample because of their properties (ULIRGs or interacting pairs), or because they had measured thermal radio fractions. The radio data were extensively and exhaustively cross-checked with many other radio catalogs, and were found to agree to within 20% in most cases. Galaxies with highly contentious radio fluxes (by more than a factor of three) were removed from the sample.

How does sample selection affect my results? Clearly, the

sample is selected very inhomogeneously to have FUV, IR and (as much as possible) radio data. This makes the effects of sample selection difficult to assess. I would argue that the effects of sample selection are minimal in this paper, partially because of the inhomogeneously-selected sample. In particular, care was taken to include both normal and starbursting galaxies across a wide range in luminosities, limiting that particular source of bias. Furthermore, the trends (or lack thereof) explored in this paper are established over 4–5 orders of magnitude in galaxy luminosity, and are impressively *quantitatively* consistent with other datasets which were selected in totally independent ways (see, e.g., Wang & Heckman 1996; Yun et al. 2001; Price & Duric 1992). Taken together, this argues for a minimal rôle for selection effects in driving the results of this paper, although further work with independently-selected samples in the future (for example, from the *Galaxy Evolution Explorer* or *Space Infrared Telescope Facility*) will prove to be the ultimate test of selection effects and systematic error in this and other investigations of the radio–IR correlation.

2.3. Comparing TIR/FUV with $H\alpha$ -derived extinctions

The crucial parameter of interest at this point is the opacity of dust to the FUV light of a given galaxy. Therefore, the vital question that must be addressed is to what level can IR/FUV be said to represent the true FUV opacity? This question is difficult to address directly; however, a number of papers have examined IR/FUV indirectly, in some detail. Meurer, Heckman, & Calzetti (1999) show that it correlates well with a number of other extinction indicators for starburst galaxies. Gordon et al. (2000) use radiative transfer models to show IR/FUV’s robustness at a theoretical level. Bell et al. (2002) shows that it correlates well with other extinction indicators for Large Magellanic Cloud H II regions. Finally, Buat et al. (2002) show correlations between IR/FUV and Balmer-derived $H\alpha$ attenuation, and show a relatively good correspondence between IR+FUV SF rates and attenuation-corrected $H\alpha$ -derived SF rates.

A galaxy’s true SF rate is impossible to measure without using detailed, complete stellar color-magnitude diagrams. Thus, I must approach this question using an indirect two-pronged approach (similar to that of Buat et al. 2002), where I intercompare SF rate indicators. First, I compare $H\alpha$ attenuation with TIR/FUV for galaxies with estimates of $H\alpha$ attenuation as a sanity check. Then, I compare SF rates derived using extinction-corrected $H\alpha$ against TIR+FUV (essentially extinction-corrected FUV) to assess how well the SF rates match.

I derive $H\alpha$ attenuations in two ways. *i*) The ratio of thermal radio to $H\alpha$ light is a known constant, to first order, therefore deviations in that ratio give a robust constraint on the $H\alpha$ attenuation. The thermal radio fraction is estimated by fitting the radio spectral energy distribution with contributions from thermal and non-thermal emission. However, the non-thermal emission dominates at most radio frequencies, making a robust and reliable determination of thermal radio flux highly challenging at this time (Condon 1992). *ii*) The Balmer decrement ($H\alpha/H\beta$) is again constant to first order in the absence of dust, and is easier to measure, but suffers from optical depth effects (see, e.g., Caplan & Deharveng 1986; Bell & Kennicutt 2001; Bell et al. 2002, for fuller discussions of these issues). Despite the substantial limitations of both techniques, I choose to compare the TIR and FUV with attenuations derived using both approaches because the goal is to assess the efficacy of

TIR/FUV: corrupted $H\alpha$ attenuation estimates will only make the TIR/FUV look worse.

I take Balmer decrements for 14 starburst galaxies with diameters $< 1.5'$ from Calzetti et al. (1994), and supplemented these with Balmer decrement measurements for two of Goldader et al.’s ULIRGs (Wu et al. 1998). For normal galaxies, I use thermal radio-derived $H\alpha$ extinctions, and some Balmer decrements which have been averaged over a number of H II regions in each galaxy (taken from Bell & Kennicutt 2001). Thermal radio fluxes were taken from Niklas et al. (1997) for 6 Rifatto et al. galaxies, and from Bell & Kennicutt (2001) for 12 UIT and two FAUST galaxies (most of their thermal radio fractions, were, in turn, from Niklas et al. 1997).

The results are shown in Fig. 1. Panel *a*) of Fig. 1 shows the comparison of $H\alpha$ attenuation and TIR/FUV (this is similar to panel *b*) of Bell & Kennicutt’s (2001) Fig. 4, and Buat et al.’s (2002) Fig. 2). In common with those studies and Calzetti et al. (1994), I find that $H\alpha$ attenuation and TIR/FUV are correlated with scatter, and that the $H\alpha$ attenuation is $\sim 1/2$ of the FUV attenuation (though with much scatter). Note that the expectation from a dust foreground screen model is that $H\alpha$ attenuation would be $\sim 1/4$ of the FUV attenuation. This discrepancy of a factor of two from the screen model is consistent with the interpretation of Calzetti et al. (1994), who postulate that nebular line emission is attenuated by roughly twice as much dust as the stellar continuum (see also Charlot & Fall 2000).

Of course, it is not clear, *a priori*, what a correlation between $H\alpha$ and FUV attenuations really tells us. One can easily imagine pathological dust geometries which will essentially decouple $H\alpha$ and FUV attenuation. A complementary, and perhaps more stringent, test is to compare attenuation-corrected $H\alpha$ -derived SF rates with SF rates determined from the combined TIR+FUV emission (essentially the same as extinction correcting FUV with TIR/FUV). Statistically, these SF rates should be equal, even though the timescales of $H\alpha$ and FUV emission differ by nearly an order of magnitude (5 Myr vs. 50 Myr). This comparison is conservative: although I know that the $H\alpha$ extinction corrections are deficient in both random and systematic ways, I nevertheless attribute any mismatches to TIR+FUV in an effort to constrain the accuracy of the TIR+FUV methodology.

A comparison of TIR+FUV SF rates and attenuation-corrected $H\alpha$ -derived SF rates is shown in panel *b*) of Fig. 1. SF rates are estimated using the SF rate conversion factors given by Kennicutt (1998). Normal galaxies with thermal radio-derived $H\alpha$ attenuations (circles) have statistically equal SF rates derived from the TIR+FUV and $H\alpha$, with less than a factor of two scatter. Normal galaxies with Balmer-derived $H\alpha$ attenuations (crosses) have statistically equal SF rates (TIR+FUV vs. $H\alpha$) also, with a factor of 1.5 scatter. Starburst galaxies and ULIRGs (stars) have SF rates which are a factor of two higher in TIR+FUV than in the Balmer attenuation-corrected $H\alpha$, with again less than a factor of two scatter. It is unclear, at this stage, why starbursting galaxies appear to have lower Balmer-corrected $H\alpha$ -derived SF rates (compared to the TIR+FUV case) than normal galaxies. This offset was also observed by Buat et al. (2002). This may be an aperture effect (FUV and extinction-corrected $H\alpha$ are in the *IUE* aperture, whereas the TIR is total), although there is no trend in TIR+FUV/ $H\alpha$ with galaxy size. Alternatively, it is possible that differences in star/dust geometry could cause an effect of this type (Buat et al. 2002), as there are strong suspicions that the

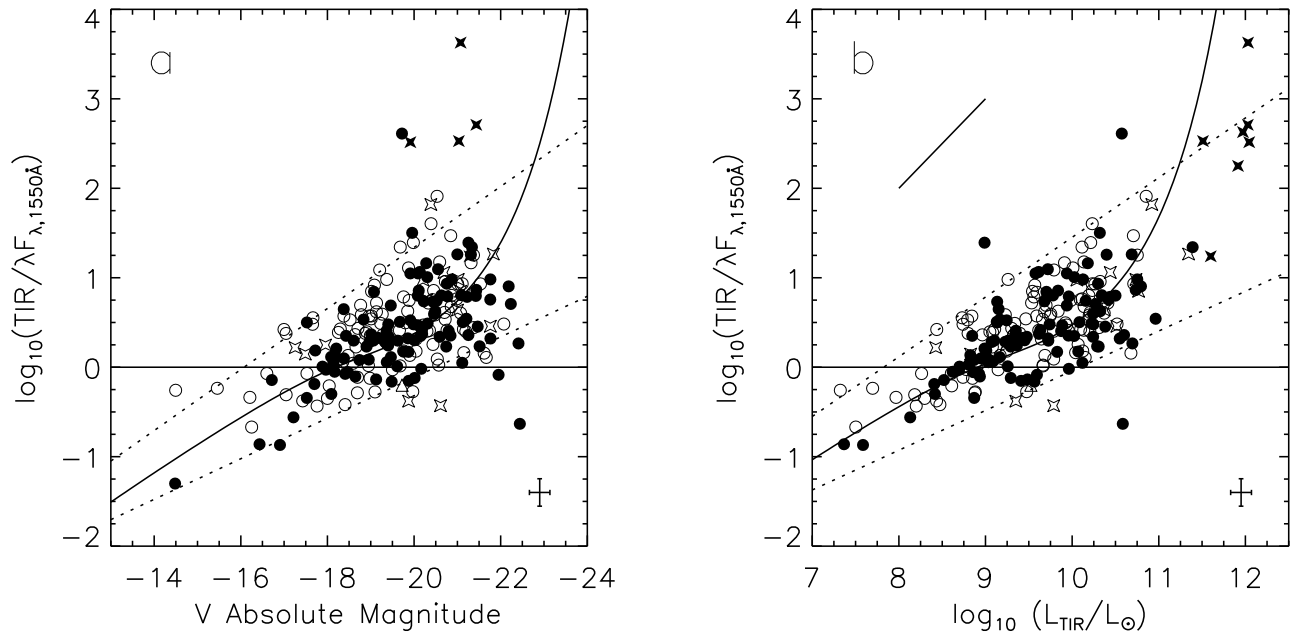


FIG. 2.— Trends in TIR/FUV with galaxy luminosity. Panel *a*) shows TIR/FUV as a function of optical *V* band luminosity. Panel *b*) shows TIR/FUV as a function of TIR luminosity. Symbols are as in Fig. 1. A single BCD is also plotted (with FUV data from Rifatto, Longo & Capaccioli 1995b) as an open triangle. Dotted lines delineate the locus of the data points in panel *a*), and are translated into panel *b*) using the *V* band–TIR correlation discussed in the text. The solid line is the model FUV opacity–luminosity correlation (driven by the gas density–luminosity and metallicity–luminosity correlations). The short solid line in panel *b*) is the effect of an order of magnitude increase in TIR luminosity at fixed FUV luminosity. Non-detections are not plotted here; see, e.g., Fig. 1 of Wang & Heckman (1996) for a version of panel *b*) which includes TIR non-detections (showing that galaxies have TIR/FUV ~ 0.1 down to $L_{\text{TIR}} \sim 10^6 L_{\odot}$).

star/dust geometries of the two galaxy types are different (Bell 2002). It is also possible that integrated galaxy spectra (as used for starbursts and ULIRGs) systematically underestimate the true $\text{H}\alpha$ attenuation because of radiative transfer effects and/or contamination from diffuse ionized gas. Without more Balmer decrement and thermal radio data for a reasonably-sized sample of starburst and normal galaxies it is impossible to unambiguously track down the origin of this factor-of-two discrepancy.

Either way, this comparison is extremely encouraging: assuming very conservatively that *all* of the scatter in TIR+FUV vs. $\text{H}\alpha$ SF rates is from the TIR and FUV (and not from the $\text{H}\alpha$ extinction correction, intrinsic differences in FUV/ $\text{H}\alpha$ because of bursts of SF, mismatches in the FUV, IR and $\text{H}\alpha$ SF rate calibrations, etc.), I find that TIR/FUV reflects the attenuation in the FUV to better than a factor of two in both a random and a systematic sense, and is perhaps much more accurate.³

2.4. Trends in TIR/FUV

I have argued that TIR/FUV is the FUV attenuation indicator of choice on both modeling and observational bases. Now, following, e.g., Wang & Heckman (1996), Buat et al. (1999), and Adelberger & Steidel (2000) I proceed to explore TIR/FUV for my diverse sample of galaxies. I show the correlation between TIR/FUV and optical luminosity, and TIR/FUV and TIR luminosity, in panels *a*) and *b*) of Fig. 2. There is a scattered but strong correlation between the ratio of total TIR 8–1000 μm to FUV (defined as λF_{λ} at $\sim 1550\text{\AA}$) and luminosity in either the

³Later on I examine the rôle of old stellar populations in heating the dust, correcting the TIR for a contribution from the optical *V* band light from a galaxy. Including this effect in this analysis does not significantly affect the conclusions; TIR/FUV is still found to be a good attenuation indicator to much better than a factor of two in a systematic and random sense.

optical *V* band or in the IR.

The dotted lines encompass the majority of the points in panel *a*), and translate into panel *b*) using the least-squares regression of TIR on *V*-band absolute magnitude: $\log_{10}(\text{TIR}/L_{\odot}) = 9.83 - 0.511M_V$. The solid line shows a highly simplistic model which links *V*-band luminosity and the optical depth of dust in the FUV. The main assumptions are that: *i*) the dust-to-gas ratio is proportional only to the metallicity, and *ii*) the dust optical depth is proportional to the dust per unit area, which therefore is proportional to the gas surface density. The dust optical depth increases with galaxy luminosity because of the typically higher gas densities and metallicities of more luminous galaxies. Curvature in the model behavior primarily comes from my somewhat crude derivation of the gas density–luminosity correlation (which is bootstrapped from the gas fraction–luminosity and stellar surface density–luminosity correlations). The model is discussed in more detail in Appendix B.

It is clear that TIR/FUV increases, on average, by over 1.5 orders of magnitude between low-luminosity galaxies at $V \sim -16$ ($L \sim 1/100L_*$) and high-luminosity galaxies at $V \sim -22$ ($L \sim 3L_*$). These data are quantitatively consistent with (largely) independently-selected samples of galaxies (e.g., Wang & Heckman 1996; Buat et al. 1999; Adelberger & Steidel 2000). The main advantage of this sample is its size: it is slightly larger than the local samples of Wang & Heckman (1996), Buat et al. (1999), and Adelberger & Steidel (2000) combined. It is interesting to note that this increase in dust opacity is reasonably well-tracked, in the mean, by the simple model which was presented above. Furthermore, while $\text{TIR}/\text{FUV} \gg 1$ for most high-luminosity galaxies, for lower-luminosity galaxies $\text{TIR}/\text{FUV} \lesssim 1$, meaning that many low-luminosity galaxies are

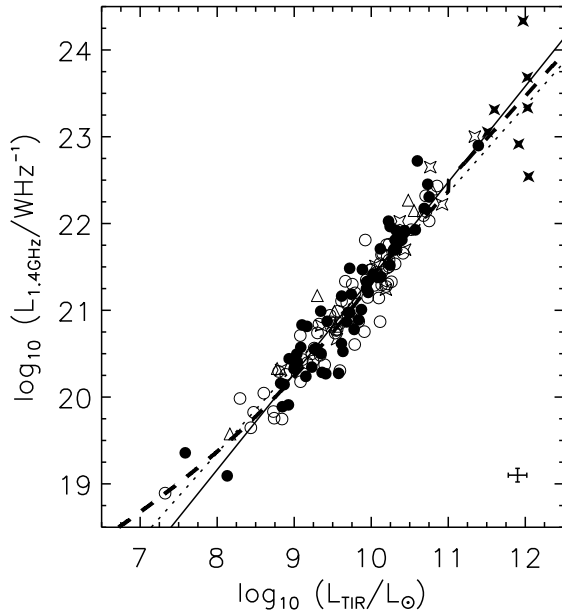


FIG. 3.— The radio–IR correlation for a total of 162 galaxies. Normal, star-forming galaxies are plotted using circles (filled circles are from UIT and FAUST, and open circles are from Rifatto, Longo & Capaccioli 1995b). Intensely star forming galaxies are denoted by stars (filled stars are ULIRGs and open stars are starbursts). A comparison sample of BCDs are shown as open triangles. A representative error bar is shown in the bottom right-hand corner. Forward and bisector fits to the data are shown by dotted and solid lines respectively. The thick dashed line shows the trend predicted by the final SF rate calibrations (see §6.1).

optically thin in the FUV. Thus, the IR luminosity in low-luminosity galaxies will underestimate the SF rate substantially (remember that TIR+FUV is not a bad proxy for SF rate; §2.3).

3. THE EFFECTS OF DUST OPACITY ON THE RADIO–IR CORRELATION

Assuming that radio is a ‘perfect’ SF rate indicator (i.e. radio \propto SF rate), the systematic depression of IR emission in low-luminosity galaxies should be easily visible in the radio–IR correlation, because of its tightness. In this section, I assess the effects of the optically-thin low-luminosity galaxies on the radio–IR correlation.

3.1. The Radio–IR correlation

The radio–IR correlation for all of the sample galaxies (plus BCDs from Hopkins et al. 2002, shown as open triangles, to check for consistency with other galaxy types) is shown in Fig. 3, where the TIR 8–1000 μ m extrapolated flux is being used. It is clear that the radio–IR correlation is both superbly tight (the scatter in the TIR/radio ratio is 0.26 dex, or less than a factor of two) and nearly linear. A forward fit, the ordinary least squares regression of TIR on radio, yields a slope of 1.05 ± 0.04 (this type of fit is suitable for, e.g., predicting the radio flux given the TIR flux). A bisector fit, the average of the forwards and backwards fits, yields a slope of 1.10 ± 0.04 (this type of fit is more suitable in cases where the intrinsic correlation is being sought, and measurement errors are dominated by intrinsic scatter; Isobe et al. 1990). These data are consistent with the much larger sample of 1809 galaxies studied by Yun et al. (2001): they recover a forward fit slope of 0.99 ± 0.01 and a scatter of 0.26 dex for a comparison of 60 μ m and 1.4 GHz fluxes. Furthermore, they find a tendency for low-luminosity galaxies to

be somewhat underluminous in the radio, which I also recover (this is the main effect which drives the slightly steeper slope of the bisector fit).

A few points deserve mention at this stage. Firstly, there is a somewhat increased dispersion for very high luminosity galaxies. This is consistent with a number of other studies (e.g., Condon et al. 1991; Yun et al. 2001; Bressan et al. 2002) and is discussed later in §6.2. Secondly, I use TIR 8–1000 μ m extrapolated flux. In this respect, I differ from most other studies which plot either the 60 μ m luminosity (e.g., Yun et al. 2001), or the FIR 42.5–122.5 μ m luminosity (e.g., Cox et al. 1988; Condon et al. 1991; Xu et al. 1994). This difference in IR luminosity estimation technique does not change the slope or scatter of the radio–IR correlation significantly (the forward fit slope for the 60 μ m case is 1.01 ± 0.04 , 42.5–122.5 μ m case is 1.04 ± 0.04 , and the scatter is 0.25 dex in all cases).

3.2. Consequences of trends in IR/FUV with galaxy luminosity

A complementary way of examining the radio–IR correlation is by constructing the TIR/radio ratio q_{TIR} . The quantity q_{TIR} is defined as:

$$q_{\text{TIR}} = \log_{10} \left(\frac{\text{TIR}}{3.75 \times 10^{12} \text{W m}^{-2}} \right) - \log_{10} \left(\frac{S_{1.4\text{GHz}}}{\text{W m}^{-2} \text{Hz}^{-1}} \right), \quad (1)$$

where $S_{1.4\text{GHz}}$ is the 1.4 GHz radio flux (e.g., Condon et al. 1991). I define q_{TIR} as the ratio of the *total* 8–1000 μ m IR luminosity to the radio power, as opposed to the 42.5–122.5 μ m FIR luminosity which is usually used in defining q . The median value of q_{TIR} is 2.64 ± 0.02 for 162 galaxies with IR and radio data and no signs of AGN, and the scatter is 0.26 dex. For reference, the median q value defined using the 42.5–122.5 μ m flux is 2.36 ± 0.02 , with a scatter of 0.26 dex, in excellent agreement with the mean q of 2.34 ± 0.01 and scatter of 0.26 dex of Yun et al. (2001).

I show the trends in q_{TIR} with galaxy luminosity in Fig. 4. Panel *a*) shows q_{TIR} as a function of *V*-band absolute magnitude, and panel *b*) shows q_{TIR} against TIR luminosity. The shaded region shows the ‘running’ upper and lower quartiles of the data⁴. There are only gentle trends, if any, in q_{TIR} with galaxy luminosity, such that lower luminosity galaxies have somewhat higher values of q_{TIR} (this is particularly visible in the q_{TIR} –TIR luminosity relation). This slight tendency for lower-luminosity galaxies to have somewhat higher q_{TIR} is what drives the slight non-linearity in the bisector fit of the radio–IR correlation, and was also seen by Yun et al. (2001) in their sample of 1809 galaxies.

This slight trend towards higher q_{TIR} at lower luminosity, or lack of trend, is in stark contrast to the trends in q_{TIR} which would be expected *if radio were a perfect SF rate indicator*. In Fig. 2, the dotted lines outlined the locus of the majority of the data points, and the solid line described the overall trend in TIR/FUV with galaxy luminosity reasonably well. The thin solid and dotted lines in Fig. 4 are the mapping of the trend in TIR/FUV with luminosity onto q_{TIR} , assuming only that the radio \propto SF rate (the details of the translation are discussed in Appendix B). If radio \propto SF rate, then q_{TIR} should decrease by at least 0.2 dex over the luminosity range over which there are decent statistics. This decrease is not seen: in fact, a slight increase in q_{TIR} with decreasing luminosity is observed. Given

⁴For a given galaxy’s luminosity, the q_{TIR} values of the ± 10 galaxies in the luminosity ranked list were extracted. The upper and lower quartile were calculated, and plotted as the shaded region.

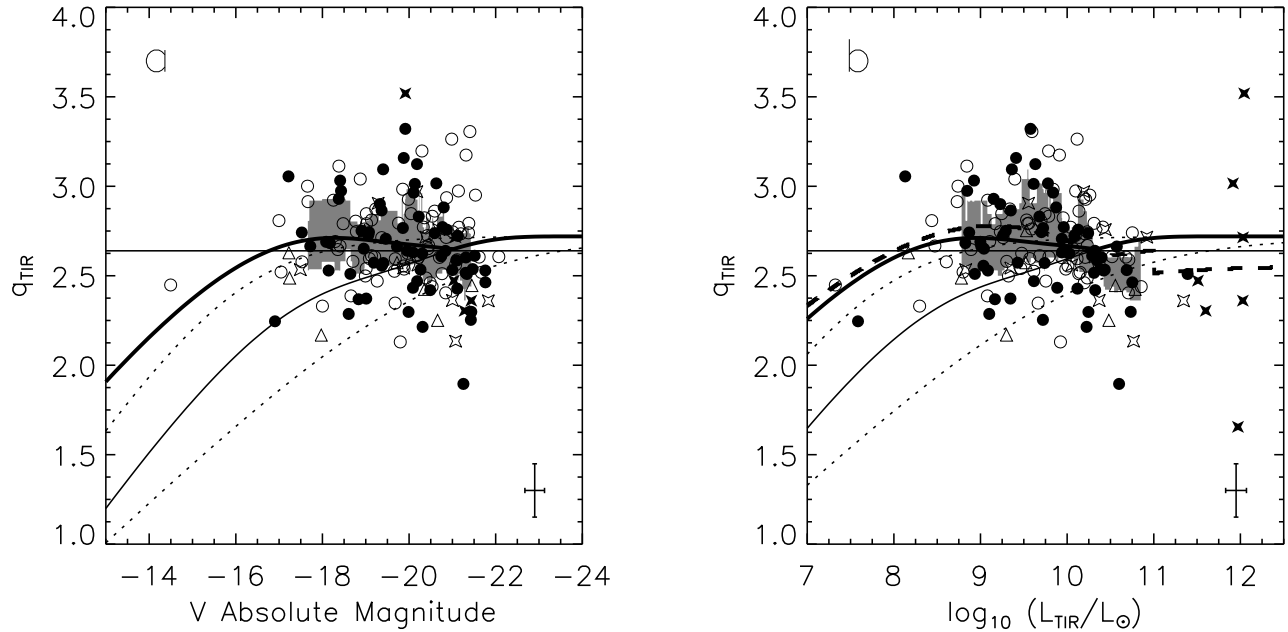


FIG. 4.— Trends in q_{TIR} with galaxy luminosity. Panel *a*) shows q_{TIR} against V -band absolute magnitude, and panel *b*) shows q_{TIR} against TIR luminosity. Symbols are the same as in Fig. 2. The shaded area shows the upper and lower quartiles as a function of luminosity: this shows, in a less noisy fashion, any trends between q_{TIR} and galaxy luminosity. The effect of trends in TIR/FUV with luminosity are plotted as thin dotted (the limits on TIR/FUV as a function of luminosity) and thin solid (the model TIR/FUV with luminosity) lines. If radio SFR were a perfect SF rate indicator, there should be a trend in q_{TIR} which follows the general trend of the thin dotted and solid lines. The thick solid line shows the final model presented in §5. The thick dashed line in panel *b*) shows the trend predicted by the final SF rate calibrations (see §6.1).

i) the robustness of TIR/FUV as an attenuation indicator (§2.3) and *ii*) the strength of the trend in TIR/FUV (§2.4) and *iii*) the fact that this trend has been observed by many other workers (e.g., Wang & Heckman 1996; Buat et al. 1999; Adelberger & Steidel 2000), it is inescapable that q_{TIR} must decrease with decreasing luminosity. The fact that it doesn't is a clear argument that *radio luminosity does not directly reflect SF rate*.

4. THE CONTRIBUTION FROM OPTICAL LIGHT FROM OLD STARS

There is an important source of uncertainty which has been neglected, however. While it is argued that the bulk of the light which is reprocessed into the IR comes from the FUV (Buat & Xu 1996; Misiriotis et al. 2001), there is nonetheless the potential for a significant contribution from older stellar populations.

4.1. A simple model for IR emission

To decompose the IR emission of the sample galaxies into contributions from old and young stellar populations, I use a simple model to interpret the FUV, V -band and IR data. In essence, the energy in the FUV, V -band and IR is balanced (assuming a constant FUV to V band dust opacity ratio) to estimate the fraction of FUV and V band light reprocessed into the IR. Thus, this approach is conceptually similar to (but more simple than) the model explored by Buat & Xu (1996).

Simplistically, I assume that all of the light in the FUV comes from the young stellar population, and that all the light in the optical V band comes from the older stellar population. I then link the optical depth in the V band to the optical depth in the FUV; $\tau_V = c\tau_{\text{FUV}}$, where c is a constant. For Milky-Way type dust and the Calzetti et al. (1994) attenuation curve the ratio between V band optical depth and $\sim 1550\text{\AA}$ optical depth is 0.4,

and for Small Magellanic Cloud Bar-type dust the ratio is closer to 1/4. However, dust is preferentially clumped around younger stars (e.g., Calzetti et al. 1994; Zaritsky 1999; Zaritsky et al. 2002), which would tend to decrease c . Taken together, a value of $c \lesssim 0.3$ is reasonable; I choose $c = 0.25$. Note that adopting a higher value of $c = 0.4$ does not significantly affect any of my conclusions (the average contribution from V -band light rises from 31% with a 16% scatter to 44% with a 18% scatter).

The observed luminosities are $L_{\text{FUV,obs}} = \lambda F_{\lambda,\text{FUV}}$ and $L_{V,\text{obs}} = \lambda F_{\lambda,V}$, where F_{λ} is the observed monochromatic luminosity at a given wavelength. Given the above assumption that $\tau_V = c\tau_{\text{FUV}}$ and denoting the FUV optical depth as τ for brevity, the intrinsic luminosities are related to the observed ones by $L_{\text{FUV,obs}} = e^{-\tau} L_{\text{FUV,intrinsic}}$ and $L_{V,\text{obs}} = e^{-c\tau} L_{V,intrinsic}$. Thus, the energy absorbed, and re-emitted into the IR is:

$$L_{\text{TIR}} = (1 - e^{-\tau})L_{\text{FUV,obs}}e^{\tau} + (1 - e^{-c\tau})L_{V,\text{obs}}e^{c\tau}. \quad (2)$$

This equation was then solved using an IDL implementation of Brent's method (Press et al. 1992, p. 352) to find the root of the equation, given the observed L_{TIR} , $L_{\text{FUV,obs}}$ and $L_{V,\text{obs}}$.

As examples, it is interesting to take S0–Sa galaxies and Scd–Sm galaxies from Popescu et al. (2002). Their S0–Sa template has a FUV: V :TIR ratio of 1:25:3 (roughly), corresponding to a fraction from V band light of 86% (calculated by multiplying the V luminosity by $c = 0.25$, and dividing by the sum of itself and the FUV flux; in this case $0.25 \times 25 / [0.25 \times 25 + 1] \sim 0.86$). In contrast, their Scd–Sm template has a FUV: V :TIR ratio of 1:2:1, corresponding to a fraction from V band light of 33%. Notwithstanding the fact that not all V band light is generated by old stellar populations, this simple analysis fits in well with what is known about the relative old stellar heating fraction as a function of galaxy type (e.g., Sauvage & Thuan 1992).

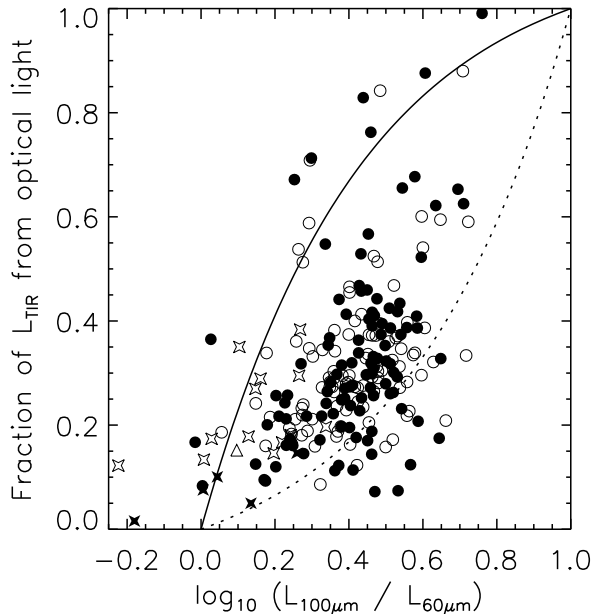


FIG. 5.— Comparison of FUV/optical/TIR-derived old stellar population contribution to the TIR luminosity against dust temperature as probed by the $100\mu\text{m}$ -to- $60\mu\text{m}$ ratio. Symbols are as in Fig. 2. Overplotted are the expected relationship between the fraction of luminosity from old stars at $60\mu\text{m}$ against dust temperature (dotted line) and the fraction of luminosity from old stars at $100\mu\text{m}$ against dust temperature (solid line).

4.2. Comparison with dust temperatures

It is instructive to compare the fraction of L_{TIR} which is plausibly associated with old stellar populations (by comparison of the amount of optical, FUV and TIR light) with the dust temperatures (which are often used as indicators of the contribution of older stellar populations to the IR luminosity). In Fig. 5, it is clear that there is a scattered correlation between the fraction of the L_{TIR} which is from optical light (which I associate then with old stellar populations) and the $100\mu\text{m}$ -to- $60\mu\text{m}$ flux ratio (where both are expressed as flux per unit frequency). Galaxies with rather larger contributions from V -band light tend to have somewhat larger $100/60$ than galaxies with a small contribution from V -band light.

It is interesting to estimate the fraction of IR light from old stellar populations which is implied by the $100/60$ observations. Estimation of a *total* fraction of the $8\text{-}1000\mu\text{m}$ luminosity from old stars using the FIR color-based technique is challenging, because of the contributions from the mid-infrared and from wavelengths longer than $\sim 120\mu\text{m}$: thus I show the contributions at $60\mu\text{m}$ (dotted line) and $100\mu\text{m}$ (solid line) from the old population as a rough guide. The cold population was assumed to have $100/60$ of 10, and the warm dust a $100/60$ of 1, following Fitt et al. (1988). Fig. 5 shows that there is good overall agreement between the expectations of the FUV/optical/TIR energy balance estimate of the contribution of old stellar populations, and the FIR color. Interestingly, this method *independently* gives further credence to FIR color-based analyses, at least at the factor-of-two level.

4.3. Correcting for the contribution of old stars as a function of luminosity

I show trends in the contribution to L_{TIR} made by old stellar populations as a function of V -band and TIR luminosity in pan-

els *a*) and *b*) of Fig. 6 respectively. It is clear that the scatter in the contribution of old populations is large at most galaxy luminosities. However, in panel *a*) of Fig. 6 there is a clear general trend of increasing old stellar population contribution with increasing V -band luminosity (albeit with large scatter). One could argue that this trend is a selection effect as galaxies with larger V -band luminosity may have larger V -band/FUV luminosity, and therefore have a larger old fraction. However, the correlation between old fraction and dust temperature (Fig. 5) argues against this interpretation, as the trend in old fraction would persist even if $60/100$ were shown against V -band luminosity (these are, of course, independent). Thus, this reflects the real and well-known observation that more optically-luminous galaxies tend to have rather older stellar populations, in the mean (e.g., Peletier & de Grijs 1998; Bell & de Jong 2000; Boissier et al. 2001; Kauffmann et al. 2003b).

Panel *b*) of Fig. 6 shows the fraction of L_{TIR} from old stellar populations against TIR luminosity. At very low luminosities, the old fraction increases with increasing galaxy luminosity. However, at $L_{\text{TIR}} \sim 10^{10}L_{\odot}$ the old fraction decreases with increasing L_{TIR} . This reflects the increasing fraction of dusty, intensely star-forming galaxies towards the highest L_{TIR} . The scatter around this general behavior is large, however.

In Fig. 7 I show the effect that the old stellar population correction has on trends in TIR/FUV with galaxy luminosity. There are some modest changes: as expected, the trend in TIR/FUV with V -band luminosity slightly flattens. However, on the whole, there is very little change in TIR/FUV with luminosity. This is, to a certain extent, for an obvious reason. A 30% change in TIR luminosity is not going to significantly affect a trend which sees a factor of $\gtrsim 30$ increase in TIR/FUV with a factor of 1000 luminosity increase. In order to significantly affect this trend, the old fraction would have to increase from essentially 0 to $\gtrsim 95\%$ over the luminosity range of interest, with relatively little scatter. This kind of behavior is clearly ruled out by the observations. Thus, the conclusion that dust opacity should leave an easily observable signature in the radio-IR correlation remains unchanged.

I check this directly in Fig. 8. When corrected for the contribution of older stellar populations, q_{TIR} decreases by a median amount of 0.16 dex while the scatter decreases slightly to 0.25 dex. The relative constancy of q_{TIR} with luminosity persists (compare Figs. 4 and 8). Again, there is a slight hint of a slightly higher q_{TIR} for lower-luminosity galaxies. Also, the ‘bump’ in q_{TIR} at $L_{\text{TIR}} \sim 10^{10}L_{\odot}$ which was reasonably apparent in panel *b*) of Fig. 4 has been largely eliminated by the correction for the old stellar population. This ‘bump’ was from a larger old fraction in earlier-type galaxies with reasonably high V -band luminosities but lower SF rates (see panel *b*) of Fig. 6). At lower luminosities, later-types dominate, and at higher IR luminosities, ULIRGs and star-bursting galaxies tend to dominate. Thus, the reasonably complete removal of this ‘bump’ feature can be taken as independent evidence that the correction for the effects of older stellar populations is doing its job reasonably well.

It is clear then that *neither* the TIR/FUV vs. luminosity correlation *nor* the q_{TIR} vs. luminosity correlation are significantly affected by the contribution of old stellar populations. Furthermore, this conclusion does not depend on the technique used to estimate the contribution from the old stellar populations, as demonstrated by the correlation between $100/60$ and the fraction of light from V -band light.

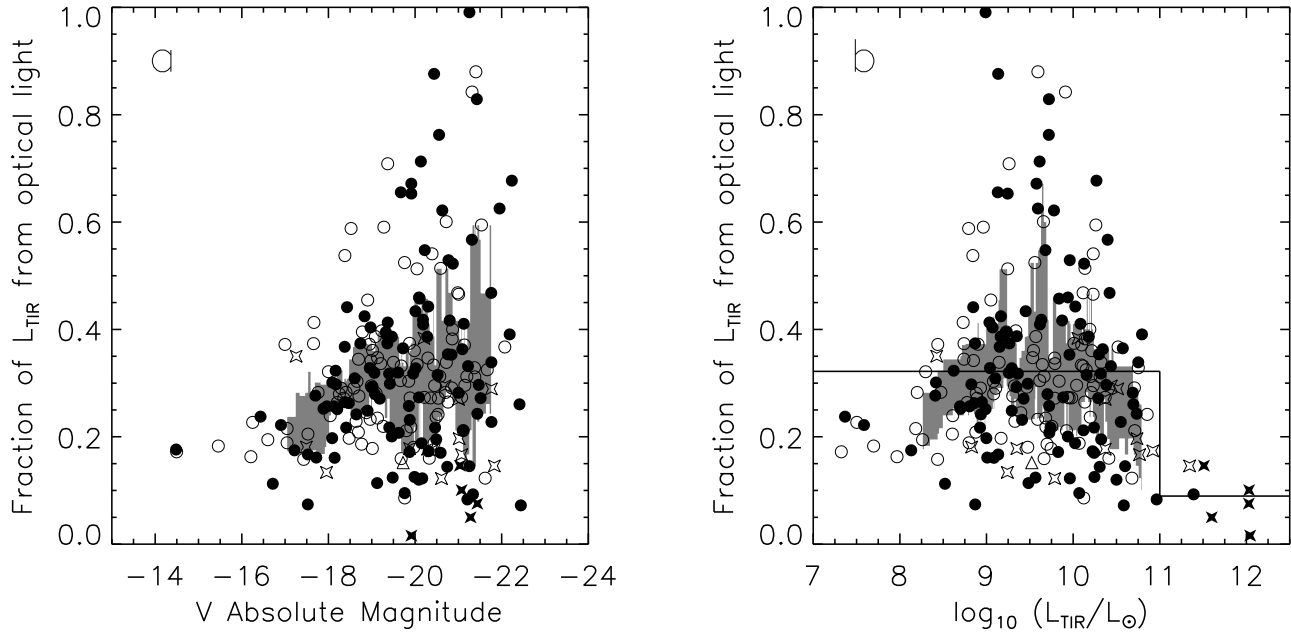


FIG. 6.— Trends in contribution to TIR luminosity from old stellar populations with galaxy luminosity in the V -band (panel a) and in the TIR (panel b). The symbols are as in Fig. 2. The shaded area shows the upper and lower quartile of the old stellar population contribution as a function of luminosity. The solid line in panel b is the average contribution from old stellar populations to L_{TIR} for galaxies above and below $10^{11}L_{\odot}$.

5. UNDERSTANDING THE RADIO EMISSION FROM GALAXIES

In §§3 and 4, I demonstrated that, if radio emission \propto SF rate, then the TIR-to-radio ratio q_{TIR} should decrease by at least a factor of two when going from $\sim L_*$ to $\sim 0.01L_*$ galaxies, owing to the effects of dust optical depth. Furthermore, accounting for old stellar populations does not affect this result. One is therefore left in the situation where a factor-of-two offset has to be there, but it isn't seen. This implies that the *radio emission of low-luminosity galaxies is suppressed, by at least a factor of two*.

Furthermore, it is the non-thermal radio emission which must be suppressed in low-luminosity galaxies. The radio emission from normal (non-active) galaxies comes from two sources. Thermal radio emission from ionized hydrogen directly tracks the SF rate (because the amount of ionized hydrogen reflects the ionizing luminosity of the very young stellar populations which are rich in massive stars). In contrast, it has been suggested for nearly 20 years that the non-thermal synchrotron emission of low-luminosity galaxies can be significantly suppressed (Klein, Wielebinksi & Thuan 1984; Klein 1991; Klein et al. 1991; Price & Duric 1992, although the thermal contribution can be very challenging to reliably estimate; Condon 1992). This can be explained in a number of ways, as the physics which links the SF rate with non-thermal emission is complex, and involves the cosmic ray production rate, galaxy magnetic field strength, and galaxy size to name just a few of the many variables (Chi & Wolfendale 1990; Helou & Bicay 1993; Lisenfeld et al. 1996). For example, Chi & Wolfendale (1990) discuss a model in which the non-thermal emission from low-luminosity galaxies is strongly suppressed, because most of the cosmic-ray electrons escape from the galaxy due to their small sizes (although the size of the effect that they predict is a factor of 3–5 in excess of the trend allowed by these observations).

Because of the complex and uncertain physics involved, I do not attempt to construct detailed theoretical model for the non-thermal radio emission. Rather, I use the data to guide me in constructing how non-thermal radio emission must track the SF rate (cf. Price & Duric 1992). I parameterize the total radio emission as $R = (n + 0.1)\eta\psi$, where R is the radio flux at 1.4 GHz, ψ is the SF rate, η is the constant of proportionality linking the SF rate and radio flux for $\sim L_*$ galaxies, and n is the relative amount of non-thermal emission. For a $\sim L_*$ galaxy, 90% of the radio flux at 1.4 GHz is non-thermal (Condon 1992), and 10% is thermal (which gives the value of 0.1). I allow n to decrease as a function of galaxy luminosity:

$$n = \begin{cases} 0.9 & L > L_* \\ 0.9(L/L_*)^{0.3} & L \leq L_* \end{cases} \quad (3)$$

where L_* is taken to be $V = -21$. The resulting relationship between q_{TIR} and luminosity is shown in Figs. 4 and 8 as thick solid lines: this variation in non-thermal radio emission accounts reasonably well for the lack of a trend in q_{TIR} with luminosity.

Remarkably, given the uncertainties inherent to decomposing the contribution of thermal/non-thermal emission from radio spectra alone, the kind of suppression of non-thermal radio emission which is required to produce a luminosity-independent q_{TIR} is consistent with an independent analysis by Price & Duric (1992). They used multi-frequency radio data to construct the radio–IR correlation at a number of frequencies. They found that the radio–IR correlation at high frequency (where thermal radio emission dominates) was nearly linear, and the radio–IR correlation at lower frequencies (where non-thermal emission dominates) was steeper. They suggested that thermal emission \propto the SF rate ψ , but suggested that non-thermal emission $\propto \psi^{1.2}$. Thus the non-thermal-to-SF rate ratio varied as $\psi^{0.2}$. Thus, for a decrease in galaxy luminosity by a factor of 100, the non-thermal-to-SF rate ratio decreases by a factor of

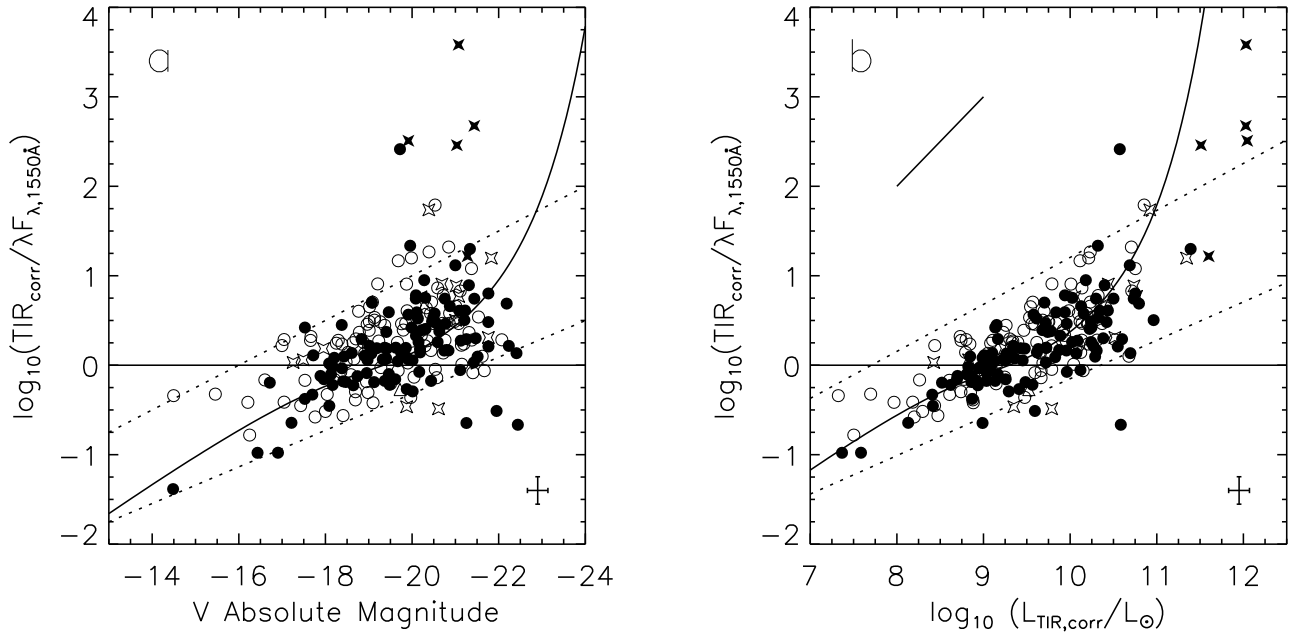


FIG. 7.— Trends in TIR/FUV with galaxy luminosity, corrected for the contribution from old stellar populations. The panels and symbols are as in Fig. 2.

2.5. Equation 3 predicts a factor of ~ 3 decrease in the non-thermal-to-SF rate ratio for the same luminosity range. Thus, the conclusion that low-luminosity galaxies have lower non-thermal contributions has been established in two independent ways: through multi-frequency radio observations (e.g., Klein et al. 1991; Price & Duric 1992, which, however, depend on uncertain radio spectral fitting) and through a lack of curvature in the radio–IR correlation (this work, which does not depend on the fitting of radio spectra in any way).

A prediction of this model is an overall correlation between galaxy luminosity and thermal radio fraction. Testing this prediction in detail is challenging because of observational difficulties. Typically, four or five radio fluxes at a range of frequencies are used to derive a non-thermal slope (which may, itself, vary with radio frequency; Condon 1992) and thermal fraction, as well as the overall normalization (Condon 1992; Niklas et al. 1997). These difficulties lead to a large uncertainty in the thermal fraction, which for the well-documented case of M82, leads to a factor of five discrepancy between different estimates of thermal fraction (Condon 1992). Notwithstanding these difficulties, I plot my prediction for thermal radio fraction from Equation 3 against observed thermal radio fractions for my sample galaxies and a further dozen non-active galaxies from the Klein et al. (1991) and Niklas et al. (1997) in Fig. 9. Clearly, most of the thermal fraction determinations are for galaxies within 1 magnitude of L_* , and are consistent with a value of 0.1 (as argued by Condon 1992). There are only a few low-luminosity galaxies in this sample, and they have a large scatter between thermal fractions of 0.1 and 1. This huge scatter should not be over-interpreted, as there are hints that it is largely intrinsic. For example, Yun et al. (2001) show that the scatter at the low-luminosity end of the radio–IR correlation is larger than for $\sim L_*$ galaxies, and it is not unreasonable to attribute some of that scatter to the radio (and therefore non-

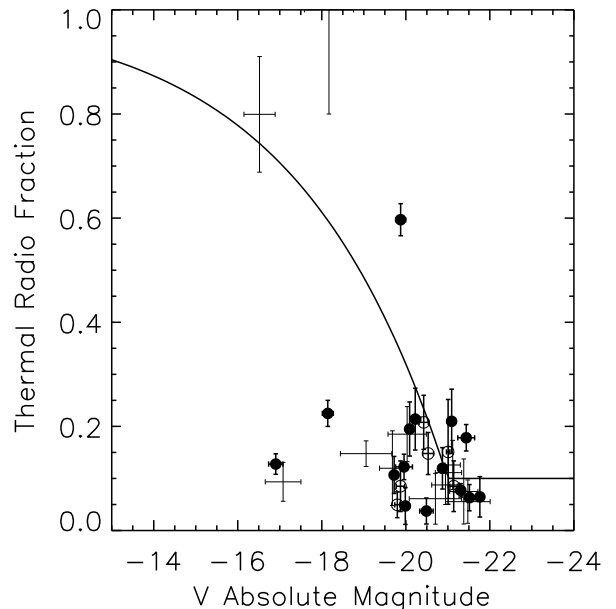


FIG. 9.— Comparison of thermal fraction at 1.4 GHz with V -band absolute magnitude. Symbols are as in Fig. 2. An additional seven non-active galaxies from Niklas et al. (1997) and five galaxies from Klein et al. (1991) are also included, plotted as error bars. Equation 3 is overplotted as a solid line.

thermal) flux.⁵ Given the modest sample size, the observational difficulty, and possibly substantial intrinsic scatter it is fair to say that my non-thermal radio calibration is not inconsistent with the thermal radio fraction data, and is strongly supported by the linearity of the radio–IR correlation and the frequency dependence in the radio–IR correlation as reported by Price &

⁵I do not see this effect in Figs. 3, 4 or 8, which is likely due to small number statistics.

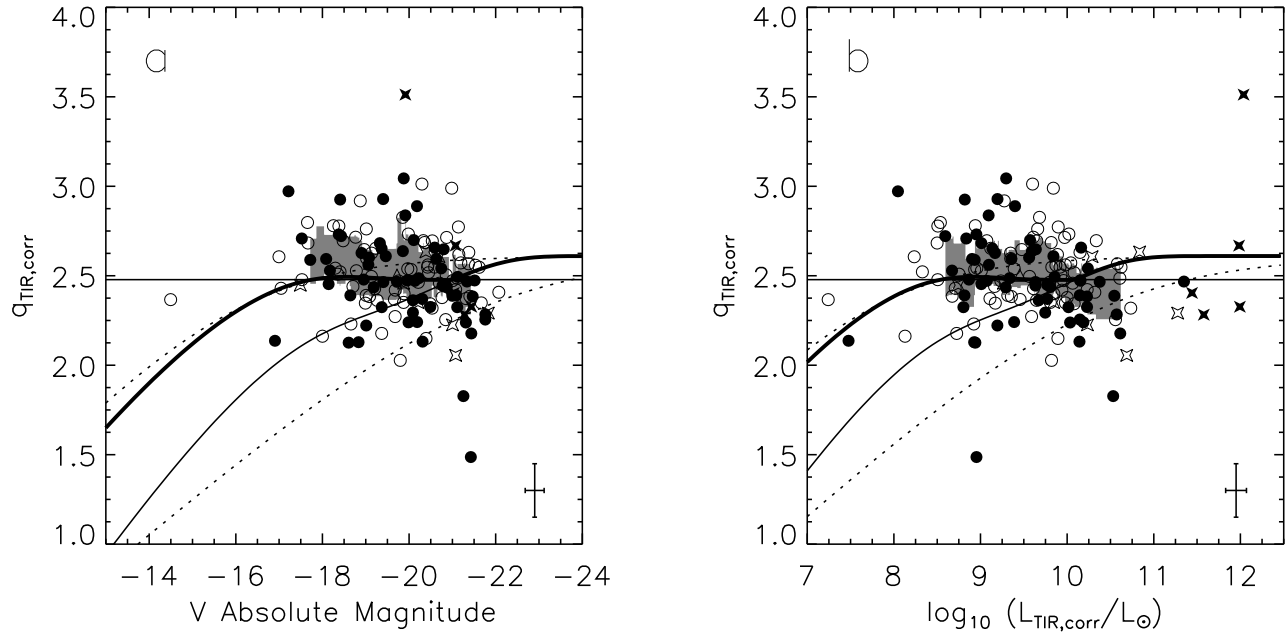


FIG. 8.— Trends in q_{TIR} with galaxy luminosity, where q_{TIR} has been corrected for the contribution from older stellar populations. The panels and symbols are the same as in Fig. 4.

Duric (1992).

6. DISCUSSION

6.1. Implications for Radio- and IR-derived SF rates

In this paper, I have brought together a diverse and wide range of literature data and interpretation into a coherent picture. On one hand, I examine the luminosity dependence in FUV (e.g., Wang & Heckman 1996; Buat et al. 1999; Adelberger & Steidel 2000; Buat et al. 2002) and $\text{H}\alpha$ attenuation (e.g., Hopkins et al. 2001; Sullivan et al. 2001), showing that low luminosity galaxies with $L \sim L_*/100$ are optically-thin in the FUV, whereas $\sim L_*$ galaxies are optically-thick in the FUV (this result is robust to the inclusion of the effects of old stellar populations). On the other hand, I show that the radio-IR correlation is nearly linear (e.g., Yun et al. 2001), and shows no sign of the expected depression of the TIR luminosity of the largely optically-thin dwarf galaxies. This means that the radio is also suppressed in dwarf galaxies (cf. Klein 1991). Since the thermal radio emission \propto SF rate, the non-thermal must depend non-linearly on SF rate: Price & Duric (1992) find that non-thermal radio emission $\propto \psi^{1.2}$, which is consistent with my data. Thus, the radio-IR correlation is linear not because both radio and IR emissions track SF rate, but rather because both radio and IR emissions fail to track SF rate in independent, but coincidentally quite similar, ways.

In this section, I use this increased understanding of the radio-IR correlation to derive TIR and radio SF rate calibrations which take into account the broad-brush suppression of TIR and radio emission from low-luminosity galaxies. Furthermore, because the scatter in TIR/FUV and q_{TIR} are well-characterized, the scatter in these SF rate calibrations will be quantified. For the purposes of a simple-to-apply SF rate calibration, and given that the scatter in FUV opacity and q_{TIR} at a given luminosity is considerable, it is sufficient to calibrate for

first-order variations in opacity and non-thermal radio emissivity in a very simple fashion (not using, e.g., the model for dust opacity developed in Appendix B). Furthermore, I will present calibrations of the SF rates simply in terms of the TIR or radio luminosity. This allows workers to derive SF rates from one flux alone while still being able to account for the reduced efficiency of TIR and radio emission from low-luminosity galaxies. If more luminosities are available (e.g. TIR, radio, optical and FUV), then a fuller analysis of the data would clearly prove superior to these simple-minded calibrations.

6.1.1. Calibrating IR-derived SF rates

In §2.3, I showed that attenuation-corrected $\text{H}\alpha$ -derived SF rates and TIR+FUV SF rates were consistent to at least a factor of two, when the SF rate calibrations of Kennicutt (1998) were adopted. Thus, I adopt the ‘starburst’ calibration of IR luminosity presented by Kennicutt (1998) for luminous $L \gtrsim L_*$ galaxies. A reasonably acceptable fit to panel *b*) of Figs. 2 and 7 is $\text{TIR}/\text{FUV} \sim \sqrt{L_{\text{TIR}}/10^9 L_\odot}$. Thus, adopting a Salpeter IMF from 0.1 to $100 M_\odot$ following Kennicutt (1998), the SF rate ψ is:

$$\psi(M_\odot \text{yr}^{-1}) = 1.72 \times 10^{-10} L_{\text{TIR}} (1 + \sqrt{10^9/L_{\text{TIR}}}), \quad (4)$$

where L_{TIR} is in solar luminosities and is calculated between 8–1000 μm (where I have adopted a solar luminosity of 3.9×10^{26} W). Note however that there is a ~ 0.5 dex scatter about this correlation, which will translate into $\pm 50\%$ scatter in the SF rate calibration at $10^9 L_\odot$, and a $\pm 20\%$ scatter at $10^{11} L_\odot$.

This calibration does not account for contributions from old stellar populations. Fig. 6 demonstrates that a correction for old stellar populations will be statistical at best. However, it is possible to correct for the mean contribution from old stellar populations in a relatively robust manner. At TIR luminosities $\leq 10^{11} L_\odot$, the mean fraction and scatter are $32\% \pm 16\%$, and

the mean fraction and scatter are $9\% \pm 5\%$ at TIR luminosities $> 10^{11} L_{\odot}$ (see the solid line in panel *b*) of Fig. 6). Thus, the final calibration, correcting for old stellar populations, is:

$$\psi(M_{\odot} \text{yr}^{-1}) = \begin{cases} 1.57 \times 10^{-10} L_{\text{TIR}} (1 + \sqrt{10^9/L_{\text{TIR}}}) & L_{\text{TIR}} > 10^{11} \\ 1.17 \times 10^{-10} L_{\text{TIR}} (1 + \sqrt{10^9/L_{\text{TIR}}}) & L_{\text{TIR}} \leq 10^{11}. \end{cases} \quad (5)$$

Expected scatter around this correlation is at least 50% at $10^9 L_{\odot}$, and 25% at $10^{11} L_{\odot}$. There are data down to $L_{\text{TIR}} \sim 10^7 L_{\odot}$; however, this calibration should be applied with *extreme* caution at such low luminosities because of the $\gtrsim 10\times$ extrapolation involved. There may be as much as a factor of two uncertainty globally, although the overall calibration uncertainty is probably somewhat less (see §2.3). Obviously, there will be uncertainties because of IMF, etc. (see Kennicutt 1998, for more discussion). It is important to realize that this calibration is certainly suspect on a galaxy-by-galaxy basis: indeed, Fig. 6 shows that there are galaxies with anywhere between 1% and 99% of their IR emission from old stellar populations.

It is interesting to note in passing that the above calibration is within a factor of two of a constant TIR conversion factor of 1.72×10^{-10} for galaxies with luminosities in excess of $\gtrsim 3 \times 10^8 L_{\odot}$. On one hand, the SF rate calibration is reduced by 10%–30% by the contribution of old stellar populations. However, on the other hand, the reduction in dust opacity with decreasing luminosity cancels out the effects of old stellar populations to first order until one reaches luminosities $\lesssim 10^9 L_{\odot}$, where the opacity is so low that the heating of dust by old stars does not significantly help. This argument was essentially made by Inoue (2002) from a more model-based standpoint.

6.1.2. Calibrating Radio-derived SF rates

In order to calibrate the radio flux in terms of SF rates, it is necessary to *i*) estimate the zero point of the SF rate scale, and *ii*) estimate the effect of increased suppression of non-thermal radio emission for low-luminosity galaxies, making sure to recast the result in terms of radio flux.

Following the above, I make the assumption that $L \gtrsim L_*$ galaxies lose no cosmic rays, and have non-thermal radio emission that directly tracks the SF rate. Thus, I choose to calibrate the radio SF rate to match the TIR SF rate for $L \gtrsim L_*$ galaxies. The geometric mean radio power per solar luminosity of TIR for $L_{\text{TIR}} \geq 2 \times 10^{10} L_{\odot}$ galaxies is $3.12 \times 10^{11} \text{ W Hz}^{-1} L_{\odot}^{-1}$, corresponding to a q_{TIR} of 2.52. Thus, in the limit of high SF rate, a radio flux at 1.4 GHz of $1.81 \times 10^{21} \text{ W Hz}^{-1}$ is predicted per $1 M_{\odot} \text{ yr}^{-1}$. This is around a factor of two higher than the Milky Way-normalized radio SF rate calibration of Condon (1992) adapted to my adopted IMF (Haarsma et al. 2000), which is well within the factor-of-two uncertainties in the assumptions underpinning the two independent calibrations (Condon et al. 2002, also found this offset between TIR-normalized and Milky Way-normalized radio SF rate calibrations).

Adopting this zero point and the variation in non-thermal radio emission from Equation 3:

$$\psi(M_{\odot} \text{yr}^{-1}) = \begin{cases} 5.52 \times 10^{-22} L_{1.4\text{GHz}} & L > L_c \\ \frac{5.52 \times 10^{-22}}{0.1+0.9(L/L_c)^{0.5}} L_{1.4\text{GHz}} & L \leq L_c, \end{cases} \quad (6)$$

where $L_c = 6.4 \times 10^{21} \text{ W Hz}^{-1}$ is the radio luminosity at 1.4 GHz of a $\sim L_*$ galaxy ($V = -21$, or $L_{\text{TIR}} \sim 2 \times 10^{10} L_{\odot}$). The scatter in q_{TIR} of 0.26 dex implies a factor-of-two uncertainty in the application of this calibration on a galaxy-by-galaxy basis. The increased scatter for both very high and very low lumi-

osity galaxies (Fig. 3 and Yun et al. 2001, respectively) implies somewhat larger uncertainties for very high and very luminosity galaxies, perhaps as large as a factor of 5, to be conservative. Furthermore, the data run out at luminosities below $3 \times 10^{19} \text{ W Hz}^{-1}$; this calibration should be used with *extreme* caution below this luminosity. An idea of the systematic calibration uncertainty is given by the factor of two offset between my and Condon's overall zero point.

The expected radio–IR correlation, and expected trends in q_{TIR} with IR luminosity as given by these TIR and radio calibrations are shown as the thick dashed lines in Figs. 3 and 4. It can be seen that the above calibrations produce a nearly linear radio–IR correlation, while fully taking into account the non-linear effects of dust opacity, old stellar populations and the non-linear dependence of non-thermal radio flux on SF rate, at least over the range over which I have data.

6.1.3. A Pinch of Salt

It is worth discussing briefly some of the limitations and caveats of the above SF rate calibrations (Equations 5 and 6).

- AGN were explicitly excluded from this sample. Obviously, IR and radio luminosities will overestimate the SF rate if *any* calibration is blindly applied to samples of galaxies which contain AGN.
- The scatter in the above calibrations is at the factor-of-two level in terms of both systematic and random errors. Furthermore, individual galaxies can deviate substantially from the mean behavior (e.g., galaxies with 99% of their IR reprocessed from the optical, or low-luminosity galaxies with thermal radio fractions which scatter considerably from the expected trend). Thus, these calibrations should not blindly be applied on an individual galaxy basis. A comprehensive multi-wavelength analysis is required to significantly constrain the SF rate of an individual galaxy.
- This sample was selected extremely inhomogeneously. Specially-selected samples (e.g., UV-selected samples; Adelberger & Steidel 2000; Sullivan et al. 2000) may be biased (for example towards low dust opacity) and may present different behaviors from this diverse local sample.
- Blind application of these calibrations as a function of lookback time may be inappropriate. For example, it is uncertain how dust opacity, the contribution of old stellar populations to dust heating, or cosmic ray retention depend on redshift. In this context, comprehensive multi-wavelength SF rates from a variety of sources (such as the rest-frame FUV, optical emission lines, IR and radio) may help to reduce the unavoidable systematic uncertainties that plague these kinds of analyses.

6.2. Increased Scatter at Low and High IR Luminosities

I found that there was an increased scatter in the radio–IR correlation at high IR luminosities (Fig. 3, and Yun et al. 2001). In addition, low IR luminosity galaxies tend to scatter more around the radio–IR correlation (e.g., Condon et al. 1991; Yun et al. 2001), although this dataset does not show this effect, perhaps because of small number statistics. This increase in the

scatter is intrinsic: the errors are $\gtrsim 3\times$ smaller than the scatter of the data.

Bressan et al. (2002) recently discussed the increase of scatter for intensely star-forming, high IR luminosity galaxies. They presented a comprehensive model which includes stellar population synthesis, dust radiative transfer, and a simplified model of radio emission from cosmic rays generated by supernovae. They predict a strong evolution in IR-to-radio ratio q with time after an intense burst of star formation: essentially, the timescale for IR emission is shorter than the timescale for radio emission, leading to variations with a total range of $\Delta q \sim 1$ over 10^8 yr timescales. This scatter matches well the observed scatter in ULIRGs.

An increased scatter at lower luminosities could partly be due to optical depth effects: low-luminosity galaxies are largely transparent in the FUV, meaning that changes in dust opacity translate directly into large changes in q_{TIR} . However, a number of recent studies (e.g., Dohm-Palmer et al. 1998; Sullivan et al. 2000; Kauffmann et al. 2003a) have suggested significant variations in SF rate over $\sim 10^8$ yr timescales for at least some lower-luminosity galaxies. These variations would lead to scatter in q_{TIR} , from mismatches between the IR and radio emission timescales (Bressan et al. 2002). Interestingly, these variations in SF rate would lead to significant variation in the thermal radio fraction (see Fig. 5 of Bressan et al. 2002), as the thermal radio emission tracks the SF rate over ~ 5 Myr timescales, whereas the non-thermal emission arguably tracks the SF rate over $\sim 10^8$ yr timescales. This could well explain much of the scatter seen by Yun et al. (2001) at low luminosities, and underlines the need for thermal radio fractions for a large sample of low-luminosity star-forming galaxies.

7. CONCLUSIONS

I have assembled a diverse sample of galaxies from the literature with FUV, optical, IR and radio luminosities to explore the calibration of radio- and IR-derived SF rates, and the origin of the radio–IR correlation. My main conclusions are as follows.

In order to establish the efficacy of IR/FUV as an extinction indicator, I compare $H\alpha$ and 8–1000 μm TIR/FUV properties of a subsample of my galaxies. I find that $H\alpha$ and FUV attenuations loosely correlate with each other, with the $H\alpha$ attenuation being roughly half of the FUV attenuation. A foreground screen model would predict an offset of a factor of a quarter. This lends support to the claim of Calzetti et al. (1994) that the nebular extinction is roughly twice that of the stellar population of the galaxy. Furthermore, when SF rates derived from TIR+FUV and attenuation-corrected $H\alpha$ are compared, I find that they agree to better than a factor of two (random and systematic). This strongly argues that TIR/FUV will give FUV attenuation estimates which are accurate to a factor of two, and probably much better.

Having established the efficacy of TIR/FUV as a FUV attenuation indicator, I explored trends in TIR/FUV with galaxy luminosity. This ratio increases on average by over a factor of 30 between low-luminosity galaxies ($L \sim 1/100L_*$) and high-luminosity galaxies ($L \sim 3L_*$). Low-luminosity galaxies have $\text{TIR/FUV} \lesssim 1$, meaning that they are *optically thin* in the FUV. Interestingly, the gross, overall trend in TIR/FUV is naturally interpreted in terms of increasing gas surface density and galaxy metallicity with increasing galaxy mass.

Like Yun et al. (2001), I find a nearly linear radio–IR correlation, with perhaps a slight tendency for faint galaxies to have a somewhat higher TIR-to-radio ratio q_{TIR} than brighter

galaxies. However, the strong and robust increase in TIR/FUV with luminosity would, if radio were a perfect SF rate indicator, produce a clear and easily measurable decrease in q_{TIR} for fainter galaxies. The data show the opposite (or no) trend, clearly demonstrating that *radio is not a perfect SF rate indicator*. Accounting for the effects of older stellar populations using a simple FUV/optical/IR energy balance model (which is consistent with FIR color-based methods) does not change this key result.

In order to cancel out the trend in q_{TIR} from optical depth effects, the non-thermal emission must be suppressed by about a factor of 2–3 in $\sim L_*/100$ galaxies relative to $\sim L_*$ galaxies. This result was also reached independently, using a totally different dataset and method, by Price & Duric (1992). Thus, the linearity of the radio–IR correlation is a conspiracy: both radio and IR underestimate the SF rate for low-luminosity galaxies.

I present SF rate calibrations which simultaneously reproduce the linearity of the radio–IR correlation, and take account of the reduced non-thermal and IR emission in lower-luminosity galaxies. However, there is considerable scatter in the SF rate calibrations, which can exceed a factor two at low galaxy luminosities. This highlights the possible influence of selection effects in interpreting the IR or radio emission from distant galaxies. Another challenge for those wishing to estimate the SF rates of distant galaxies is the non-trivial physics that links IR/radio and SF rate. For example, the evolution of dust opacity, the importance of old stellar populations, and the evolution of the efficiency of cosmic ray confinement are all essentially unconstrained as a function of lookback time. This adds considerable systematic uncertainty to our understanding of galactic SF rates in the distant Universe.

I thank Betsy Barton Gillespie, Andrew Hopkins, Rob Kennicutt, Casey Papovich and J. D. Smith for useful discussions and their comments on the manuscript. The anonymous referees are thanked for their feedback. This work was supported by NASA grant NAG5-8426 and NSF grant AST-9900789. This work made use of NASA’s Astrophysics Data System Bibliographic Services, and the NASA/IPAC Extragalactic Database (NED) which is operated by the Jet Propulsion Laboratory, California Institute of Technology, under contract with the National Aeronautics and Space Administration.

REFERENCES

- Adelberger, K. L., & Steidel, C. C. 2000, ApJ, 544, 218
- Becker, R. H., White, R. L., Helfand, D. J. 1995, ApJ, 450, 559
- Bell, E. F. 2002, ApJ, 577, 150
- Bell, E. F., de Jong, R. S. 2000, MNRAS, 312, 497
- Bell, E. F., & Kennicutt Jr., R. C. 2001, ApJ, 548, 681
- Bell, E. F., Gordon, K. D., Kennicutt Jr., R. C., Zaritsky, D. 2002, ApJ, 565, 994
- Blain, A. W., Smail, I., Ivison, R. J., & Kneib, J.-P. 1999, MNRAS, 302, 632
- Boissier, S., Boselli, A., Prantzos, N., Gavazzi, G. 2001, MNRAS, 321, 733
- Bothun, G. D., Lonsdale, C. J., Rice, W. 1989, ApJ, 341, 129
- Bottinelli, L., Gougenheim, L., Paturel, G., de Vaucouleurs, G. 1984, A&AS, 56, 381
- Bottinelli, L., Gougenheim, L., Paturel, G., Teerikorpi, P. 1986, A&A, 156, 157
- Bressan, A., Silva, L., Granato, G. L. 2002, A&A, 392, 377
- Buat, V. 1992, A&A, 264, 444
- Buat, V., Xu, C., 1996, A&A, 306, 61
- Buat, V., Deharveng, J. M., Donas, J. 1989, A&A, 223, 42
- Buat, V., Donas, J., Milliard, B., Xu, C. 1999, A&A, 352, 371
- Buat, V., Boselli, A., Gavazzi, G., Bonfanti, C. 2002, A&A, 383, 801
- Calzetti, D., Kinney, A. L., Storchi-Bergmann, T. 1994, ApJ, 429, 582
- Calzetti, D., Bohlin, R. C., Kinney, A. L., Storchi-Bergmann, T., Heckman, T. M. 1995, ApJ, 443, 136

- Caplan, J., Deharveng, L. 1986, *A&A*, 155, 297
- Charlot, S., Fall, S. M., 2000, *ApJ*, 539, 718
- Chi, X., Wolfendale, A. W. 1990, *MNRAS*, 245, 101
- Clemens, M. S., Alexander, P., Green, D. A. 1999, *MNRAS*, 307, 481
- Condon, J. J., 1992, *ARA&A*, 30, 575
- Condon, J. J., Anderson, M. L., Helou, G. 1991, *ApJ*, 375, 95
- Condon, J. J., Cotton, W. D., Greisen, W., Yin, Q. F., Perley, R. A., Taylor, G. B., Broderick, J. J. 1998, *AJ*, 115, 1693
- Condon, J. J., Cotton, W. D., Broderick, J. J. 2002, *AJ*, 124, 675
- Cox, M. J., Eales, S. A., Alexander, P., Fitt, A. J. 1988, *MNRAS*, 235, 1227
- Dale, D. A., Helou, G., Neugebauer, G., Soifer, B. T., Frayer, D. T., & Condon, J. J. 2001, *AJ*, 122, 1736
- Deharveng, J. M., Sasseen, T. P., Buat, V., Bowyer, S., Lampton, M., Wu, X., 1994, *A&A*, 289, 715
- de Jong, R. S., Lacey, C. 2000, *ApJ*, 545, 781
- de Jong, T., Klein, U., Wielibinski, R., Wunderlich, E. 1985, *A&A*, 147, L6
- de Vaucouleurs, A., Longo, G. 1988, Catalogue of visual and infrared photometry of galaxies from 0.5 micrometer to 10 micrometer (1961–1985) (Austin, University of Texas)
- de Vaucouleurs, G., de Vaucouleurs, A., Corwin Jr., H. G. Buta, R. J., Paturel, G., Fouque, P., 1991, Third Reference Catalogue of Bright Galaxies, version 3.9 (New York, Springer Verlag) (RC3)
- Devereux, N. A., Eales, S. A. 1989, *ApJ*, 340, 708
- Dohm-Palmer, R. C., et al. 1998, *AJ*, 116, 1227
- Doublier, V., Comte, G., Petrosian, A., Surace, C., Turatto, M. 1997, *A&AS*, 124, 405
- Ekholm, T., Lanoix, P., Teerikorpi, P., Fouqué, P., Paturel, G. 2000, *A&A*, 355, 835
- Ferreras, I., Silk, J. 2001, *ApJ*, 557, 165
- Fitt, A. J., Alexander, P., Cox, M. J. 1988, *MNRAS*, 233, 907
- Flores, H., et al. 1999, *ApJ*, 517, 148
- Garcia-Baretto, J. A., Franco, J., Guichard, J., Carrillo, R. 1995, *ApJ*, 451, 156
- Gavazzi, G., Boselli, A. 1996, *ApL&C*, 35, 1
- Gavazzi, G., Boselli, A. 1999a, *A&A*, 343, 86
- Gavazzi, G., Boselli, A. 1999b, *A&A*, 343, 93
- Gavazzi, G., Boselli, A., Scodreggio, M., Pierini, D., Belsole, E. 1999, *MNRAS*, 304, 595
- Goldader, J. D., Meurer, G., Heckman, T. M., Seibert, M., Sanders, D. B., Calzetti, D., Steidel, C. C. 2002, *ApJ*, 568, 651
- Gordon, K. D., Clayton, G. C., Witt, A. N., Misselt, K. A. 2000, *ApJ*, 533, 236
- Haarsma, D. B., Partridge, R. B., Windhorst, R. A., Richards, E. A. 2000, *ApJ*, 544, 641
- Han, M. 1992, *ApJS*, 81, 35
- Helou, G., & Bica, M. D. 1993, *ApJ*, 415, 93
- Helou, G., Khan, I. R., Malek, L., Boehmer, L. 1988, *ApJS*, 68, 151
- Hopkins, A. M., Connolly, A. J., Haarsma, D. B., Cram, L. E. 2001, *AJ*, 122, 288
- Hopkins, A. M., Schulte-Ladbeck, R. E., Drozdovsky, I. O. 2002, *AJ*, 124, 862
- Inoue, A. K. 2002, *ApJ*, 570, 97L
- Isobe, T., Feigelson, E. D., Akritas, M. G., Babu, G. J. 1990, *ApJ*, 364, 104
- Jansen, R. A., Franx, M., Fabricant, D., Caldwell, N. 2000, *ApJS*, 126, 271
- Karachentsev, I. D., et al. 2002, *A&A*, 385, 21
- Karachentsev, I. D., Makarova, D. A. 1996, *AJ*, 111, 794
- Kauffmann, G., et al. 2003a, *MNRAS*, submitted (astro-ph/0204055)
- Kauffmann, G., et al. 2003b, *MNRAS*, submitted (astro-ph/0204070)
- Kennicutt Jr., R. C. 1998, *ARA&A*, 36, 189
- Kennicutt Jr., R. C., Kent, S. M., 1983, *AJ*, 88, 1094
- Kennicutt Jr., R. C., Keel, W. C., van der Hulst, J. M., Hummel, E., Roettiger, K. A., 1987, *AJ*, 93, 1011
- Kinney, A. L., Bohlin, R. C., Calzetti, D., Panagia, N., Wyse, R. F. G. *ApJS*, 86, 5
- Klein, U. 1991, *PASAu*, 9, 253
- Klein, U., Wielebinski, R., Thuan, T. X. 1984, *A&A*, 141, 241
- Klein, U., Weiland, H., Brinks, E. 1991, *A&A*, 246, 323
- Lauberts, A., Valentijn, E. A., 1989, The Surface Photometry Catalogue of the ESO-Uppsula Galaxies (Garching bei München, ESO)
- Lee, M. G., Kim, M., Sarajedini, A., Geisler, D., Gieren, W. 2002, *ApJ*, 565, 959
- Li, A., Draine, B. T. 2001, *ApJ*, 554, 778
- Lisenfeld, U., Völk, H. J., Xu, C. 1996, *A&A*, 314, 745
- Lonsdale Persson, C. J., Helou, G. 1987, *ApJ*, 314, 513
- Macri, L. M., et al. 1999, *ApJ*, 521, 155
- Maddox, S. J., Sutherland, W. J., Efstathiou, G., Loveday, J. 1990, *MNRAS*, 243, 692
- Makarova, L. N., Karachentsev, I. D., Georgiev, Ts. B. 1997, *AstL*, 23, 378
- Mann, R. G., et al. 2002, *MNRAS*, 332, 549
- Mas-Hesse, J. M., Dunth, D. 1999, *A&A*, 349, 765
- Mathewson, D. S., Ford, V. L. 1996, *ApJS*, 107, 97
- Matthews, L. D., Wood, K. 2001, *ApJ*, 548, 150
- McGaugh, S. S., de Blok, W. J. G. 1997, *ApJ*, 481, 689
- Meurer, G. R., Heckman, T. M., & Calzetti, D. 1999, *ApJ*, 521, 64
- Misiriotis, A., Popescu, C. C., Tuffs, R. J., Kylafis, N. D. 2001, *A&A*, 372, 775
- Moshir, M., et al., 1990, IRAS Faint Source Catalogue, version 2.0 (Pasadena, IPAC)
- Niklas, S. 1997, *A&A*, 322, 29
- Niklas, S., Klein, U., Wielebinski, R. 1997, *A&A*, 322, 19
- Pagel, B. E. J. 1998, “Nucleosynthesis and Chemical Evolution of Galaxies” (Cambridge University Press, Cambridge)
- Peletier, R. F., de Grijs, R. 1998, *MNRAS*, 300, 3L
- Popescu, C. C., Misiriotis, A., Kylafis, N. D., Tuffs, R. J., Fischera, J. 2000, *A&A*, 362, 138
- Popescu, C. C., Tuffs, R. J., Völk, H. J., Pierini, D., Madore, B. F. 2002, *ApJ*, 567, 221
- Press W. H., Teukolsky S. A., Vetterling W. T., Flannery B. P., 1992, “Numerical Recipes in Fortran 77: The Art of Scientific Computing” (Cambridge University Press, Cambridge).
- Price, R., Duric, N. 1992, *ApJ*, 401, 81
- Rice, W., Lonsdale, C. J., Soifer, B. T., Neugebauer, G., Kopan, E. L., Lloyd, L. A., de Jong, T., Habing, H. J. 1988, *ApJS*, 68, 91
- Rifatto, A., Longo, G., Capaccioli, M. 1995a, *A&AS*, 109, 341
- Rifatto, A., Longo, G., Capaccioli, M. 1995b, *A&AS*, 114, 527
- Romanishin, W. 1990, *AJ*, 100, 373
- Sakai, S., et al. 2000, *ApJ*, 529, 698
- Sanders, D. B., Mirabel, I. F. 1996, *ARA&A*, 34, 749
- Sauvage, M., Thuan, T. X. 1992, *ApJ*, 396, 69L
- Schlegel, D. J., Finkbeiner, D. P., & Davis, M., 1998, *ApJ*, 500, 525
- Shanks, T., 1997, *MNRAS*, 290, 77L
- Sheth, K., Regan, M. W., Vogel, S. N., Teuben, P. J. 2000, *ApJ*, 532, 221
- Skillman, E. D., Kennicutt Jr., R. C., Hodge, P. W. 1989, *ApJ*, 347, 875
- Sodroski, T. J., Odegard, N., Arendt, R. G., Dwek, E., Weiland, J. L., Hauser, M. G., Kelsall, T. 1997, *ApJ*, 480, 173
- Soifer, B. T., Boehmer, L., Neugebauer, G., Sanders, D. B. 1989, *AJ*, 98, 766
- Spinoglio, L., Malkan, M. A., Rush, B., Carrasco, L., Recillas-Cruz, E. 1995, *ApJS*, 453, 616
- Sullivan, M., Treyer, M. A., Ellis, R. S., Bridges, T. J., Milliard, B., Donas, J. 2000, *MNRAS*, 312, 442
- Sullivan, M., Mobasher, B., Chan, B., Cram, L., Ellis, R., Treyer, M., Hopkins, A. 2001, *ApJ*, 558, 72
- Takamiya, M., Kron, R. G., Kron, G. E. 1995, *AJ*, 110, 1083
- Teerikorpi, P., Bottinelli, L., Gougenheim, L., Paturel, G. 1992, *A&A*, 260, 17
- Tikhonov, N. A., Karachentsev, I. D. *A&AS*, 128, 325
- Tonry, J. L., Dressler, A., Blakeslee, J. P., Ajham, E. A., Fletcher, A. B., Luppini, G. A., Metzger, M. R., Moore, C. B. 2001, *ApJ*, 546, 681
- Tuffs, R. J., et al. 2002, *ApJS*, 139, 37
- Tully, R. B., Shaya, E. J. 1984, *ApJ*, 281, 31
- van Zee, L., Haynes, M. P., Salzer, J. J. 1997, *AJ*, 114, 2479
- Vila-Costas, M. B., Edmunds, M. G. 1992, *MNRAS*, 259, 121
- Walterbos, R. A. M., Greenawalt, B. 1996, *ApJ*, 460, 696
- Wang, B., Heckman, T. M., 1996, *ApJ*, 457, 645
- White, R. L., Becker, R. H. 1992, *ApJS*, 79, 331
- Whittet, D. C. B. 1992, Dust in the Galactic Environment (New York, IOP Publishing)
- Wright, A. E., Griffith, M. R., Burke, B. F., Ekers, R. D. 1994, *ApJS*, 91, 111
- Wu, H., Zou, Z. L., Xia, X. Y., Deng, Z. G. 1998, *A&AS*, 127, 521
- Xu, C., Buat, V., Boselli, A., Gavazzi, G. 1997, *A&A*, 324, 32
- Xu, C., Lisenfeld, U., Völk, H. J., Wunderlich, E. 1994, *A&A*, 282, 19
- Yasuda, N., Fukugita, M., Okamura, S. 1997, *ApJS*, 108, 417
- Young, J. S., Allen, L., Kenney, J. D. P., Lesser, A., Rownd, B., 1996, *AJ*, 112, 1903
- Yun, M. S., Reddy, N. A., Condon, J. J. 2001, *ApJ*, 554, 803
- Zaritsky, D. 1999, *AJ*, 118, 2824
- Zaritsky, D., Kennicutt Jr., R. C., Huchra, J. P. 1994, *ApJ*, 420, 87
- Zaritsky, D., Harris, J., Thompson, I. B., Grebel, E. K., Massey, P. 2002, *AJ*, 123, 855
- Zepf, S., Lui, M. C., Marleau, F. R., Sackett, P. D., Graham, J. R. 2000, *AJ*, 119, 1701

APPENDIX

A. MULTI-WAVELENGTH PHOTOMETRY

My galaxy sample was primarily selected to have published FUV photometry at $\sim 1500\text{\AA}$. Here, I describe the sources of the FUV, optical, IR, radio, and other data, and the error estimates for each type of data. I also present my galaxy luminosities, as an aid to workers in the field, in Table A1.

FUV Data

The FUV data at wavelengths $\sim 1550\text{\AA}$ were taken from a variety of sources: UIT fluxes at an average wavelength of 1567\AA for normal spiral and dwarf galaxies from Bell & Kennicutt (2001), 1495\AA IUE fluxes for UV-bright starbursts from Calzetti et al. (1994, 1995), 1650\AA STIS data from the *Hubble Space Telescope* for a sample of ULIRGs from Goldader

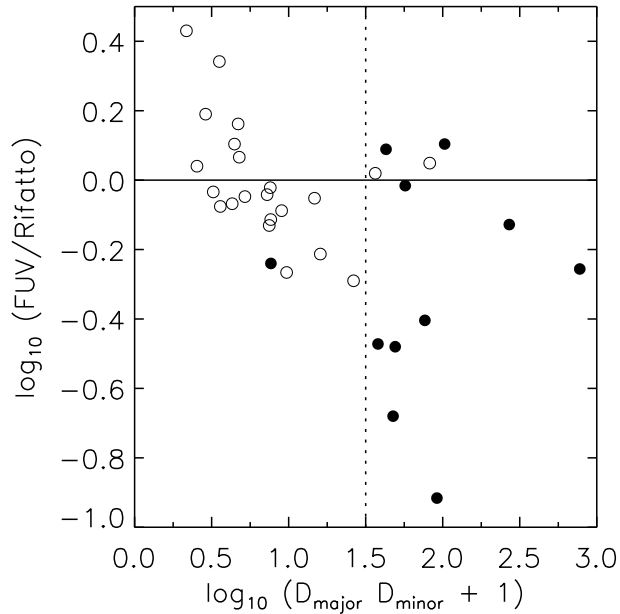


FIG. A10.— A comparison of FAUST (22 galaxies; open circles) and UIT (11 galaxies; filled circles) FUV flux with those from Rifatto, Longo & Capaccioli (1995b). The solid line denotes no offset between fluxes, and the dotted line represents the size cut applied to galaxies from Rifatto, Longo & Capaccioli (1995b): galaxies with $\log_{10}(D_{\text{major}}D_{\text{minor}} + 1) \geq 1.5$ are omitted from the sample.

et al. (2002), 1650Å fluxes from normal galaxies from the FAUST experiment by Deharveng et al. (1994), and large-aperture 1650Å UV fluxes from a variety of UV experiments which were homogenized and extrapolated to total by Rifatto, Longo & Capaccioli (1995a,b).

Error estimates for the different sources of data are as follows.

- UIT and FAUST were shown to be consistent to within 20% (=0.08 dex) by Bell & Kennicutt (2001).
- IUE fluxes for this sample are also accurate to ~ 0.08 dex (Kinney et al. 1993).
- The STIS fluxes for the seven ULIRGs have a mean accuracy of ~ 0.12 dex (Goldader et al. 2002).
- Fluxes from Rifatto, Longo & Capaccioli (1995b) were compiled from the literature, and so have variable quality. In Fig. A10, I show a comparison of FAUST and Rifatto, Longo & Capaccioli (1995b) fluxes (open circles), and UIT and Rifatto, Longo & Capaccioli (1995b) fluxes (filled circles) as a function of galaxy area. Rifatto, Longo & Capaccioli (1995b) sometimes substantially over-extrapolate the FUV fluxes of large galaxies: this conclusion was also reached by Bell & Kennicutt (2001) when they compared UIT and Rifatto, Longo & Capaccioli (1995b) fluxes with OAO, SCAP and FOCA data (their Fig. 1). Accordingly, all galaxies from Rifatto, Longo & Capaccioli (1995b) with $\log_{10}(D_{\text{major}}D_{\text{minor}} + 1) \geq 1.5$ are removed from the sample (29 galaxies). The remaining 21 galaxies from Rifatto, Longo & Capaccioli (1995b) with UIT or FAUST data and $\log_{10}(D_{\text{major}}D_{\text{minor}} + 1) < 1.5$ are consistent with a scatter of 0.19 dex. While substantial,

this scatter is consistent with the combined error estimates, and is substantially smaller than the intrinsic scatter in, e.g., the TIR/FUV correlation with total TIR luminosity, or V band absolute magnitude. In Fig. A10, there also appears to be a trend between the FAUST/UIT fluxes and Rifatto, Longo & Capaccioli (1995b) fluxes for $\log_{10}(D_{\text{major}}D_{\text{minor}} + 1) < 1.5$. A correction of either the Rifatto, Longo & Capaccioli (1995b) data, or the FAUST/UIT data for this trend simply increases scatter in TIR/FUV at a given TIR or V -band luminosity, and is therefore not applied.

The IUE spectroscopic aperture is $10'' \times 20''$ in size. Accordingly, to minimize aperture effects I choose to use the FUV data for starburst galaxies with optical diameters $\leq 1.5'$ only. Tests have shown that this diameter cutoff excludes all of the galaxies with truly obvious aperture effects (e.g., gross mismatches between FUV attenuations measured by TIR/FUV, which are susceptible to aperture mismatch, and UV-color based attenuations, which are impervious to aperture worries), while keeping a reasonable sample size. Larger starbursts are included in this study, but are assumed to have no FUV data (i.e. only the optical, IR and radio data are used).

The data come from wavelengths between 1450Å and 1650Å. I make the simplifying assumption that the fluxes are all measured at 1550Å. A typical star-forming galactic spectrum has $F_{\lambda} \propto \lambda^{-1}$ at these wavelengths (Bell 2002). Thus, the error introduced by this assumption is $\sim 6\%$.

As is obvious from the above discussion, there is some overlap between the different samples. I prefer FAUST/UIT FUV photometry above the Rifatto, Longo & Capaccioli (1995b) photometry in all cases. There were two galaxies which overlapped between the Rifatto, Longo & Capaccioli (1995b) sample and the starburst sample. While the Rifatto, Longo & Capaccioli (1995b) total FUV fluxes would probably be preferred (because of aperture effects in the IUE starburst data), I choose to use the IUE data for those two galaxies so that the $H\alpha$ +Balmer decrement data and FUV measurements have matched apertures. The measurements were consistent to within 0.3 dex at any rate, and adopting Rifatto, Longo & Capaccioli (1995b) fluxes for these two galaxies does not affect the results.

Optical Data

Optical data are principally taken from the Third Reference Catalogue of Bright Galaxies (RC3; de Vaucouleurs et al. 1991). Values of V_T , the total V band magnitude not corrected for extinction or inclination, were taken, when available. If necessary, V -band apparent magnitudes were estimated from B and R -band data from the ESO-LV Catalogue (Lauberts & Valentijn 1989) assuming that V is the average of B and R magnitudes (assuming an error of 0.2 mag). As a last resort, V band fluxes were estimated from RC3 B_T values, assuming $B - V \sim 0.6$ for normal galaxies (assuming an error of 0.5 mag). A more homogeneous and accurate optical magnitude would be ideal; however, magnitudes of this accuracy will be adequate for this study.

IR Data

The IR data were taken from (in order of preference) the catalog of IRAS observations of large optical galaxies (Rice et al. 1988), the IRAS Bright Galaxy Sample (Soifer et al. 1989), and the IRAS Faint Source Catalog (Moshir et al. 1990). Internal accuracy between the different catalogs is typically better

than 10%, and the true uncertainties (including zero point and calibration uncertainties) are $\sim 20\%$ (estimated by comparing ISO/IRAS cross-calibration; e.g., Tuffs et al. 2002).

The $12\mu\text{m}$, $25\mu\text{m}$, $60\mu\text{m}$ and $100\mu\text{m}$ fluxes are used to estimate total IR fluxes in two ways. The integrated $42.5\text{--}122.5\mu\text{m}$ emission is well-approximated (to a few percent) by the FIR estimator of Helou et al. (1988):

$$\text{FIR} = 1.26 \times 10^{-14} (2.58 S_{60\mu\text{m}} + S_{100\mu\text{m}}) \text{W m}^{-2}, \quad (\text{A1})$$

where $S_{60\mu\text{m}}$ and $S_{100\mu\text{m}}$ are the $60\mu\text{m}$ and $100\mu\text{m}$ fluxes in Jy. However, this definition of the FIR flux omits contributions shortwards of $42.5\mu\text{m}$ and longwards of $122.5\mu\text{m}$: both spectral regions contribute significantly to the total IR energy budget. Following Gordon et al. (2000), I estimate the total IR flux from $8\mu\text{m}$ to $1000\mu\text{m}$ by direct integration of the $12\text{--}100\mu\text{m}$ fluxes, and by extrapolating the flux longwards of $100\mu\text{m}$ using the $60\mu\text{m}$ and $100\mu\text{m}$ to define the temperature of a modified blackbody curve with a λ^{-1} emissivity. If $12\mu\text{m}$ or $25\mu\text{m}$ do not exist for a galaxy (89 and 87 galaxies out of 245, respectively), they are estimated using $f_{12\mu\text{m}}(\text{Jy}) = 0.0326 f_{100\mu\text{m}}(\text{Jy})$ or $f_{25\mu\text{m}}(\text{Jy}) = 0.131 f_{60\mu\text{m}}(\text{Jy})$, which were derived from the rest of the sample and are good to 30%. The contribution to the total IR from the mid-IR component is $\sim 20\%$, and so the total uncertainty introduced by this approximation is not large, $\lesssim 10\%$. Total IR (TIR) fluxes defined in this way are typically a factor of two higher than the FIR estimator, with an obvious dependence on the $60\mu\text{m}$ to $100\mu\text{m}$ ratio. For reference, the TIR fluxes are $\sim 30\%$ larger than the F_{IR} $8\text{--}1000\mu\text{m}$ estimator of Sanders & Mirabel (1996). I have used 150–205 *Infrared Space Observatory* (ISO) measurements of 38 Virgo Cluster galaxies (Popescu et al. 2002) to check the extrapolation of the $12\text{--}100\mu\text{m}$ fluxes using the λ^{-1} emissivity. I find that TIR estimates where the $12\text{--}170\mu\text{m}$ data are used are 10% larger than TIR estimates where the $12\text{--}100\mu\text{m}$ data are used, with a 10% scatter. Furthermore, this offset is *independent of dust temperature* between $\log_{10}(L_{100\mu\text{m}}/L_{60\mu\text{m}})$ values of 0.1 to 0.8 (which covers most of my main sample galaxies). Because the offset is modest and because the systematic errors in IR calibration are the same size or larger (Tuffs et al. 2002), I have chosen to leave my TIR values uncorrected for this offset. Note that none of my conclusions are significantly affected by this 10% offset: the TIR calibrations remain unchanged because the calibration is, to first order, model-based and the radio calibration would increase by 10% (in the sense that per unit radio flux, the SF rate will be increased by 10%) because the same radio flux must reflect the 10% increase in SF rate implied by the larger TIR flux. In this paper, I explore mostly the ratio of TIR ($8\text{--}1000\mu\text{m}$, extrapolated) fluxes with radio; however the FIR to radio ratio is also briefly explored to check for consistency with the literature. Errors in FIR and TIR are somewhat larger than the individual flux errors, and are $\sim 30\%$.

Radio Data

Radio data for 166 galaxies at 1.4 GHz were, for the most part, taken from the NRAO VLA Sky Survey (NVSS; Condon et al. 1998). NVSS data were taken for 159 galaxies from Condon et al. (2002), Hopkins et al. (2002), and Gavazzi & Boselli (1999a,b) in that order of preference. Internally, the consistency between these studies of the NVSS was $\lesssim 10\%$ for larger fluxes, and $\lesssim 1\text{ mJy}$ for fainter sources. Comparison of the NVSS fluxes with literature galaxy fluxes from other, independent data was somewhat less clean: fluxes were repeatable

to 20% or so, degrading considerably for fainter sources. Noting the superior uniformity and resolution of the NVSS, I adopt error estimates of 10% and 2 mJy, to be added in quadrature, for these 159 galaxies. I removed by hand a few galaxies which had highly discrepant (off by more than a factor of three) NVSS vs. literature fluxes, where it was unclear which radio flux was more accurate, in the interests of being as conservative as possible. Additional data at frequencies between 1.4 and 1.5 GHz (translated to 1.4 GHz assuming a $\nu^{-0.8}$ non-thermal spectrum) were taken from other sources for seven galaxies which were not in the above catalogs, but were important to have in the sample because of their properties (ULIRGs or interacting pairs), or because they had measured thermal radio fractions. These radio data were extensively cross-checked with many other radio catalogs, and were found to agree to within 20% in most cases.

Other Data

Exquisite distances are not central to the purpose of this paper, as most of the diagnostics of the behavior of the radio–IR correlation are ratios of fluxes. Nevertheless, in order to construct L_{TIR} and V -band absolute magnitudes, distances are required to the sample galaxies. Distances were taken from a variety of sources, and were scaled roughly to reflect $H_0 = 75\text{ km s}^{-1}\text{ Mpc}^{-1}$ and a distance to the Virgo and Ursa Major Clusters of 20 Mpc (e.g., Shanks 1997; Sakai et al. 2000). Typical distance uncertainties of 25% will produce absolute magnitude errors of ~ 0.5 mag, dwarfing the V -band apparent magnitude and TIR flux errors in most cases.

The galactic foreground extinction has been calculated using the models of Schlegel et al. (1998).

$\text{H}\alpha$ fluxes and attenuation estimates were required in §2.3 in order to establish the efficacy of TIR/FUV as a FUV attenuation indicator. $\text{H}\alpha$ fluxes for galaxies with $\text{H}\alpha$ attenuation estimates in the literature were taken from a variety of sources. Inter-comparison of the fluxes indicates a $\sim 20\%$ uncertainty. Thermal radio fractions were taken from Bell & Kennicutt (2001) for the UIT and FAUST galaxies (which in turn mostly come from Niklas et al. 1997), and from Niklas et al. (1997) directly for the Rifatto, Longo & Capaccioli (1995b) galaxies. Balmer decrements were taken from Calzetti et al. (1994) and Wu et al. (1998) for starburst galaxies and ULIRGs respectively. Average Balmer decrements for H II regions in the UIT and FAUST galaxies are taken from Bell & Kennicutt (2001). Thermal radio fractions and Balmer decrements are difficult to do external comparisons on in detail, because of their rarity in the literature, but there are substantial error bars attached to each type of estimate because of the difficulty of disentangling the thermal and dominant non-thermal contributions to the radio flux (discussed extensively by e.g., Condon 1992; Niklas et al. 1997) on one hand, and aperture mismatches and stellar absorption corrections, coupled with astrophysical uncertainties such as optical depth effects, on the other hand (Caplan & Deharveng 1986).

B. LINKING GALAXY LUMINOSITY WITH OPTICAL DEPTH

Observed attenuation–luminosity correlations (e.g., Wang & Heckman 1996; Buat et al. 1999; Hopkins et al. 2001) are relatively easy to understand, at least at a qualitative level, using some simple arguments. The basic argument is that the metals-to-dust ratio is constant. Then the optical depth τ depends only on gas column density and gas metallicity Z . In turn, the gas column density varies as a function of galaxy luminosity (tending to be rather higher for more luminous galaxies), and the metal-

licity is higher for more luminous galaxies. Both effects tend to drive a higher dust opacity in more luminous galaxies.

The dust opacity τ at $\sim 1550\text{\AA}$ is given by $\tau = n_d C_{\text{ext}}$ where n_d is the number of dust grains along the line of sight per unit cross section, and C_{ext} is the extinction cross section (Whittet 1992). The dust absorption cross section (which I use instead of the extinction cross section because as much light will be scattered into the line of sight as out of it) at 1550\AA is $\kappa_{\text{abs}} = 4.2 \times 10^4 \text{ cm}^2 \text{ g}^{-1}$ (Li & Draine 2001). Using this, I obtain $\tau = 8.4 \Sigma_{\text{dust}}$ where Σ_{dust} is in $M_{\odot} \text{ pc}^{-2}$. Assuming that the dust-to-metals ratio is constant ~ 0.2 (assuming solar metallicity and a gas/dust of 226; Sodroski et al. 1997), $\Sigma_{\text{dust}} = 0.2Z\Sigma_{\text{gas}}$, where Σ_{gas} is the gas density in $M_{\odot} \text{ pc}^{-2}$. However, trends in Σ_{gas} with luminosity are poorly studied. Therefore, I choose to approximate Σ_{gas} with the gas-to-stellar mass ratio multiplied by the stellar surface density Σ_* . Then, $\Sigma_{\text{dust}} = 0.2Zf_g/(1-f_g)\Sigma_*$, where f_g is the gas fraction. This crude estimation of the gas densities from the gas fraction plus the stellar densities is clearly an over-simplification; however, it is clear that the general trend of increasing dust opacity with increasing luminosity is a robust one as *both* the typically increasing metallicity and gas density with galaxy luminosity (at least for star-forming galaxies) will cause the dust opacity to increase with luminosity. I now address each luminosity-dependent variable in turn.

The origin of the strong metallicity–luminosity correlation (e.g., Skillman, Kennicutt & Hodge 1989; Vila-Costas & Edmunds 1992; Zaritsky, Kennicutt & Huchra 1994; van Zee et al. 1997; Bell & de Jong 2000) is not fully understood, but it is argued that both the greater degree of astration in more luminous galaxies, and galaxy mass-dependent metal loss play a rôle (see, e.g., Pagel 1998, for a thorough treatment of the issues). Following Fig. 16 of Bell & de Jong (2000), I adopt the following metallicity–luminosity correlation: $\log_{10}(Z/Z_{\odot}) = -0.1875 * V - 3.875$, where $Z_{\odot} = 0.02$ is the solar metallicity, V denotes V -band absolute magnitude, and I assume $V - K \sim 3$.

There is a decreasing gas fraction with increasing galaxy luminosity (e.g., McGaugh & de Blok 1997; Bell & de Jong 2000), which is easily interpreted in terms of astration. More luminous galaxies tend to have formed stars with greater efficiency (arguably because of their typically higher gas surface densities although other mechanisms are plausible; see, e.g., Bell & de Jong 2000; Ferreras & Silk 2001) and have older stellar populations and lower gas fractions, albeit with a large scatter. I adopt a gas fraction–luminosity correlation: $f_g = 0.5 + 1/\pi \arctan[0.5(V + 19)]$, where f_g is the gas fraction. This is consistent with the correlation presented by Bell & de Jong (2000).

Lastly, the stellar surface density Σ_* is known to vary smoothly with galaxy mass (de Jong & Lacey 2000; Kauffmann et al. 2003b) roughly as $\log_{10} \Sigma_* = 2.34 - 0.213(V + 21)$, assuming that the stellar M/L in V -band is roughly constant (which is wrong at only a factor of 3 level). Therefore, $\tau = 1.7\eta Z f_g / (1 - f_g) \Sigma_*$, where η is a constant of order unity that is tuned to fit the observed trend in TIR/FUV with luminosity: this constant allows me to fit out any of the crude modeling assumptions and accounts for the effects of star/dust geometry on the opacity. Note that star/dust geometry effects will tend to drive η below unity, as a star/dust mix attenuates light less per unit mass than the screen model that I have assumed. Given that the relationship between FUV attenuation τ and TIR/FUV is $\tau \sim 2.5 \log_{10}(1 + \text{TIR}/\text{FUV})$, it follows that $\log_{10}(\text{TIR}/\text{FUV}) = \log_{10}(10^{0.4\tau} - 1)$. In order to match the data reasonably well (the

solid curve in Fig. 2), I adopt $\eta = 0.7$.

In order to connect the TIR/radio ratio q_{TIR} with TIR/FUV, I assume that SF rate $\propto \text{TIR} + \text{FUV}$, and that radio is a perfect SF rate indicator. Then, $q_{\text{TIR}} = -\log_{10}\{1 + 1/(10^{0.4a\tau} - 1)\} + q_0$, where q_0 is the intrinsic TIR/radio ratio which is tuned to match the observed q_{TIR} at $\sim L_*$.

In §4, I correct the data for the effects of old stellar populations. In this case, I set $\eta = 0.5$, and change the value of q_0 to match the observed q_{corr} (the average q_{TIR} , once the TIR has been corrected for old stellar populations) at $\sim L_*$.

It is interesting to briefly note that the τ depends largely on gas column density, modulated mostly by metallicity. In the above model, the gas column density was derived in a very statistical fashion by adopting a stellar surface density–luminosity correlation (which has much intrinsic scatter), and a gas fraction–luminosity correlation (which also has a lot of intrinsic scatter). Thus, a very testable generic prediction of this type of model is that dust opacity should correlate well with a combination of gas column density and metallicity, with substantially less scatter than the correlation between opacity and galaxy luminosity. Testing this prediction in detail is far beyond the scope of this work, but it is interesting to note that low surface brightness galaxies, with a very low gas column density, tend to be relatively dust-free (e.g., Matthews & Wood 2001), and ULIRGs, with very high gas column densities, tend to be very dusty. In addition, the good correlation between FUV extinction as measured by TIR/FUV with total gas density (Buat 1992; Xu et al. 1997) is consistent with this scheme.

TABLE A1
GALAXY LUMINOSITIES

Galaxy Name	FUV ($\log_{10}[W/\text{\AA}]^{-1}$)	TIR ($\log_{10}[W]^{-1}$)	FIR _{Helou} ($\log_{10}[W]^{-1}$)	100/60	1.4 GHz ($\log_{10}[W/\text{Hz}]^{-1}$)	f_{thermal}	V (mag)	A_V (mag)	D (Mpc)	H α ($\log_{10}[W]^{-1}$)	$A_{\text{H}\alpha, \text{Balmer}}$ (mag)	Type	References
NGC 598	32.35 ± 0.04	35.63	35.36	3.00	20.40 ± 0.04	...	-18.95 ± 0.10	0.14	0.8	Scd	1a,2a,4a
NGC 628	33.00 ± 0.04	36.55	36.26	3.15	21.34 ± 0.04	...	-20.84 ± 0.10	0.23	10.0	34.17	0.84	Sc	1b ^{2a}
DDO 81	32.09 ± 0.06	34.72	34.39	4.41	19.09 ± 0.08	...	-17.22 ± 0.21	0.12	3.1	32.88	...	Sm	1b ^{2a}
DDO 50	31.85 ± 0.02	34.18	33.91	2.28	19.36 ± 0.06	0.128 ± 0.020	-16.90 ± 0.17	0.11	3.1	32.64	0.15	Im	1b ^{2a}
NGC 5457	33.45 ± 0.01	36.88	36.60	2.87	21.69 ± 0.04	0.063 ± 0.025	-21.51 ± 0.10	0.03	7.4	34.49	0.53	Scd	1b ^{2a}
NGC 5055	32.54 ± 0.04	36.72	36.36	3.94	21.39 ± 0.04	0.119 ± 0.040	-20.87 ± 0.10	0.06	7.6	33.95	1.22	Sbc	1b ^{2a}
NGC 3034	31.36 ± 0.15	37.16	36.88	1.06	21.93 ± 0.04	0.107 ± 0.036	-19.72 ± 0.09	0.54	3.3	34.12	2.82	I	1b ^{2a}
NGC 3351	31.94 ± 0.06	36.20	35.98	1.99	20.62 ± 0.05	...	-20.13 ± 0.10	0.09	9.0	33.67	0.69	Sb	1b ^{2a}
NGC 2403	32.36 ± 0.03	35.85	35.58	2.88	20.55 ± 0.04	...	-19.06 ± 0.08	0.13	3.0	33.69	0.38	Scd	1b ^{2a}
NGC 5236	32.81 ± 0.02	36.75	36.44	2.40	-20.52 ± 0.04	0.22	3.7	34.29	1.75	Sc	1b ^a
DDO 75	31.02 ± 0.04	32.91	32.63	2.63	-14.48 ± 0.11	0.15	1.4	32.09	...	Im	1b ^a
NGC 4449	32.42 ± 0.01	35.68	35.46	1.77	20.57 ± 0.04	0.225 ± 0.025	-18.14 ± 0.13	0.07	3.4	33.55	0.46	Im	1b ^{2a}
NGC 4736	32.34 ± 0.01	36.27	36.01	2.17	20.87 ± 0.04	0.214 ± 0.059	-20.22 ± 0.13	0.06	4.8	33.76	0.46	Sab	1b ^{2a}
NGC 4038/9	33.27 ± 0.01	37.32	37.09	1.69	22.45 ± 0.04	0.178 ± 0.025	-21.44 ± 0.20	0.15	19.8	34.80	0.53	Pec	1b ^{a,d}
NGC 891	...	37.03	36.72	3.25	21.92 ± 0.04	...	-20.26 ± 0.18	0.22	9.9	33.55	...	Sb	1b ^{2a}
NGC 4156	32.90 ± 0.09	21.98 ± 0.09	...	-21.70 ± 0.05	0.09	90.0	Sb	1b ^{2a}
NGC 5253	32.03 ± 0.04	35.73	35.33	0.96	-17.53 ± 0.12	0.18	3.6	33.47	0.61	Im	1b ^a
NGC 2903	32.29 ± 0.03	36.53	36.23	2.81	21.33 ± 0.04	0.195 ± 0.052	-20.09 ± 0.10	0.10	6.3	33.87	0.91	Sd	1b ^{2a}
NGC 6090	33.44 ± 0.01	37.98	37.72	1.49	22.90 ± 0.04	...	-21.34 ± 0.10	0.07	117.0	35.07	...	Pec	1b ^{2a}
NGC 3310	33.16 ± 0.01	36.84	36.60	1.40	21.97 ± 0.04	0.047 ± 0.035	-19.99 ± 0.10	0.07	13.9	34.48	...	Sbc	1b ^{2a}
NGC 4214	32.39 ± 0.02	35.52	35.30	1.63	19.91 ± 0.05	...	-18.41 ± 0.15	0.07	4.2	33.48	0.23	Im	1b ^{2a}
Mrk 66	33.29 ± 0.03	36.66	36.40	1.48	-19.76 ± 0.10	0.04	87.0	34.09	...	BCG	1b ^a
NGC 4631	33.09 ± 0.03	36.91	36.66	2.52	21.92 ± 0.04	0.037 ± 0.025	-20.49 ± 0.16	0.06	8.4	34.26	0.84	Sd	1b ^{2a}
IRAS 08339+6517	33.82 ± 0.02	37.55	37.33	1.01	-21.21 ± 0.40	0.30	76.0	35.05	...	Pec	1b ^a
NGC 925	32.96 ± 0.08	36.00	35.75	3.49	20.27 ± 0.06	0.597 ± 0.031	-19.88 ± 0.12	0.25	8.9	33.87	0.76	Sd	1b ^{2a}
NGC 1512	32.02 ± 0.04	35.72	35.44	3.50	-19.67 ± 0.10	0.03	9.8	Sab	1b ^a
NGC 1291	30.99 ± 0.11	35.58	35.22	5.76	-21.25 ± 0.04	0.04	8.6	32.66	...	S0a	1b ^a
NGC 253	32.21 ± 0.15	36.91	36.66	1.86	21.70 ± 0.04	0.122 ± 0.024	-19.96 ± 0.20	0.06	2.6	33.69	...	Sc	1b ^{a,d}
NGC 1313	32.64 ± 0.04	35.85	35.63	2.56	-19.61 ± 0.20	0.37	3.9	33.68	...	Sd	1b ^a
NGC 6946	...	36.90	36.61	2.52	21.81 ± 0.04	0.077 ± 0.013	-21.31 ± 0.11	1.15	6.2	34.42	0.69	Scd	1b ^{2a}
NGC 4321	33.06 ± 0.11	37.01	36.72	2.68	21.91 ± 0.04	...	-21.76 ± 0.08	0.09	16.0	34.33	0.38	Sbc	1b ^{2a}
UGC 6697	33.64 ± 0.05	37.19	36.92	1.89	22.72 ± 0.04	...	-21.25 ± 0.10	0.07	90.0	34.73	...	Im	1b ^{2a}
NGC 3389	32.81 ± 0.01	36.48	36.23	2.53	21.47 ± 0.05	...	-20.09 ± 0.06	0.09	24.0	34.03	...	Sc	1b ^{2a}
NGC 4647	32.41 ± 0.04	36.62	36.26	2.99	21.42 ± 0.04	...	-20.30 ± 0.08	0.09	20.0	33.87	...	Sc	1b ^{2a}
NGC 1317	32.02 ± 0.03	36.31	36.04	2.88	-20.55 ± 0.06	0.07	20.0	33.41	...	S0a	1b ^a
NGC 2993	33.10 ± 0.02	37.09	36.86	1.59	-20.09 ± 0.14	0.20	32.0	34.42	...	Sa	1b ^a
NGC 2551	31.80 ± 0.18	35.73	35.38	4.04	-20.44 ± 0.20	0.09	31.0	S0a	1b ^a
Haro 15	33.47 ± 0.04	37.11	36.80	1.45	-21.76 ± 0.20	0.07	86.7	34.49	...	Pec	1c,3a,4b,5a
IC 1586	33.03 ± 0.04	36.96	36.62	1.76	-20.29 ± 0.20	0.14	81.3	34.38	1.21	H II	1c,3a,4b,5a
IC 214	33.50 ± 0.04	37.94	37.72	1.57	23.00 ± 0.04	...	-21.83 ± 0.20	0.14	125.3	34.60	1.11	...	1c,2a,3a,4b,5a
Mrk 499	33.17 ± 0.04	37.33	36.94	2.18	-21.02 ± 0.20	0.05	98.6	34.25	0.94	Im	1c,3a,4b,5a
NGC 1510	31.62 ± 0.04	35.02	34.80	1.27	-17.25 ± 0.20	0.03	11.1	32.68	0.17	Pec	1c,3a,4b,5a
NGC 1705	...	34.62	34.40	1.89	-16.69 ± 0.20	0.02	5.9	32.35	...	Pec	3a,4b,5a ^b
NGC 1800	...	34.87	34.60	2.28	-17.09 ± 0.20	0.04	8.1	31.98	...	Im	3a,4b,5a ^b
NGC 3049	...	36.15	35.88	1.56	20.67 ± 0.09	...	-19.29 ± 0.20	0.12	20.6	33.47	...	Sab	2a,3a,4b,5a ^b
NGC 3125	32.41 ± 0.04	35.83	35.61	1.02	-17.96 ± 0.20	0.24	12.1	33.53	0.27	Sab	1c,3a,4b,5a
NGC 3256	...	38.13	37.90	1.18	-22.25 ± 0.20	0.38	37.7	34.89	...	Pec	3a,4b,5a ^b
NGC 4194	32.52 ± 0.04	37.51	37.26	1.07	22.22 ± 0.04	...	-20.39 ± 0.20	0.05	37.0	34.54	1.67	Im	1c,2a,3a,4b,5a
NGC 4385	32.53 ± 0.04	36.78	36.48	1.28	21.24 ± 0.07	...	-20.18 ± 0.20	0.08	33.1	34.13	...	S0	2a,3a,4b,5a ^b
UGC 9560	32.10 ± 0.04	35.42	35.13	1.75	20.31 ± 0.13	...	-17.49 ± 0.20	0.04	17.0	33.30	0.31	Pec	1c,2a,3a,4b,5a
NGC 5860	32.80 ± 0.04	37.03	36.77	1.84	21.70 ± 0.11	...	-20.69 ± 0.20	0.06	73.5	34.39	1.44	...	1c,2a,3a,4b,5a
NGC 5996	32.50 ± 0.04	36.65	36.40	1.85	21.51 ± 0.05	...	-20.21 ± 0.20	0.11	30.2	33.82	0.98	Sc	1c,2a,3a,4b,5a
NGC 6052	33.33 ± 0.04	37.36	37.13	1.66	22.65 ± 0.04	...	-21.08 ± 0.20	0.24	58.6	34.46	0.44	...	1c,2a,3a,4b,5a
Tololo 1924-416	33.63 ± 0.04	36.38	36.09	0.60	-20.61 ± 0.20	0.27	38.7	34.50	0.04	Pec	1c,3a,4b,5a
NGC 7250	33.15 ± 0.04	35.94	35.75	1.34	20.82 ± 0.06	...	-19.87 ± 0.20	0.47	16.6	33.52	0.19	Sdm	1c,2a,3a,4b,5a
NGC 7552	...	37.69	37.45	1.42	-21.32 ± 0.20	0.04	24.9	34.25	...	Sab	3a,4b,5a ^b
NGC 7673	33.15 ± 0.04	36.96	36.78	1.40	22.03 ± 0.05	...	-21.00 ± 0.20	0.13	45.1	34.28	0.88	Pec	1c,2a,3a,4b,5a
NGC 7714	...	36.91	36.62	1.06	21.73 ± 0.04	...	-20.04 ± 0.20	0.16	26.1	34.46	...	Sab	2a,3a,4b,5a ^b
NGC 7793	...	35.44	35.16	2.87	-18.44 ± 0.20	0.06	3.0	31.42	...	Sab	3a,4b,5a ^b
VV 114	33.79 ± 0.01	38.19	37.96	1.36	23.31 ± 0.04	...	-21.28 ± 0.30	0.05	82.8	ULIRG	1d,2b,3b,4b

TABLE A1—Continued

Galaxy Name	FUV ($\log_{10}[W/\text{\AA}]^{-1}$)	TIR ($\log_{10}[W]^{-1}$)	FIR _{Helou} ($\log_{10}[W]^{-1}$)	100/60	1.4 GHz ($\log_{10}[W/\text{Hz}]^{-1}$)	f_{thermal}	V (mag)	A_V (mag)	D (Mpc)	H α ($\log_{10}[W]^{-1}$)	$A_{\text{H}\alpha, \text{Balmer}}$ (mag)	Type	References
IRAS 08572+3915	32.96 ± 0.10	38.63	38.35	0.66	22.54 ± 0.15	...	-19.92 ± 0.50	0.09	243.0	ULIRG	1d,2c,3c,4b
IC 883	32.41 ± 0.06	38.10	37.92	1.82	23.05 ± 0.04	...	-21.03 ± 0.30	0.04	95.2	33.59	5.59	ULIRG	1d,2a,3d,4b,5b
Mrk 273	32.75 ± 0.05	38.62	38.47	1.01	23.68 ± 0.04	...	-21.44 ± 0.30	0.03	157.0	34.40	3.09	ULIRG	1d,2a,3d,4b,5b
IRAS 15250+3609	33.09 ± 0.04	38.51	38.30	0.81	22.92 ± 0.07	0.06	231.7	ULIRG	1d,2c,4b
Arp 220	31.83 ± 0.12	38.62	38.50	1.11	23.33 ± 0.04	...	-21.07 ± 0.30	0.17	74.1	32.43	...	ULIRG	1d,2a,3d,4b,5b
IRAS 19254-7245	32.77 ± 0.10	38.56	38.30	1.05	24.33 ± 0.04	0.28	255.2	ULIRG	1d,2d,4b
NGC 4592	31.87 ± 0.08	35.44	35.15	2.36	19.89 ± 0.12	...	-18.43 ± 0.30	0.07	9.8	Sdm	1e,2a,4d
PGC 043701	33.60 ± 0.08	37.14	36.85	2.69	-21.76 ± 0.05	0.31	56.4	Sb	1e,3e,4e
NGC 4930	33.05 ± 0.08	36.18	35.80	5.13	-21.95 ± 0.30	0.36	34.5	Sbc	1e,4e
NGC 4793	32.80 ± 0.08	37.28	37.00	2.24	22.17 ± 0.04	...	-21.00 ± 0.22	0.04	33.1	Sc	1e,2a,4e
IC 2050	34.59 ± 0.08	37.18	36.88	2.95	-22.44 ± 0.30	0.05	164.9	Sbc	1e,4e
NGC 1536	32.16 ± 0.08	35.46	35.11	3.47	-18.74 ± 0.14	0.07	17.3	Sc	1e,4e
IC 2073	33.03 ± 0.08	36.42	36.17	2.10	-19.87 ± 0.15	0.03	53.0	Scd	1e,4e
NGC 1602	32.15 ± 0.08	35.58	35.31	2.45	-18.20 ± 0.16	0.03	17.0	Im	1e,4e
NGC 5264	31.60 ± 0.08	33.96	33.68	2.54	-16.43 ± 0.15	0.17	4.5	Im	1e,4f
PGC 047958	33.05 ± 0.08	36.61	36.32	2.90	-20.15 ± 0.20	0.17	60.9	I	1e,3f,4e
IC 4275	33.35 ± 0.08	36.55	36.28	2.36	-20.17 ± 0.20	0.19	57.5	S	1e,3f,4e
IC 4248	33.02 ± 0.08	36.83	36.59	1.93	-20.46 ± 0.20	0.21	55.1	S	1e,3f,4e
NGC 3956	32.51 ± 0.08	36.07	35.77	2.89	-19.42 ± 0.20	0.13	21.9	Sc	1e,3f,4e
NGC 4027	32.74 ± 0.08	36.89	36.63	2.21	-20.76 ± 0.04	0.14	22.3	Sdm	1e,4e
NGC 6753	33.26 ± 0.08	37.39	37.13	2.90	-22.18 ± 0.07	0.23	41.7	Sb	1e,4e
IC 4845	32.94 ± 0.08	36.86	36.50	3.79	-22.23 ± 0.14	0.19	52.7	Sab	1e,4e
IC 4836	33.02 ± 0.08	37.03	36.73	2.92	-21.22 ± 0.13	0.18	54.8	Sc	1e,4e
IC 4819	32.29 ± 0.08	35.45	35.14	3.31	-18.47 ± 0.20	0.20	24.5	Sd	1e,4e
IC 4828	33.10 ± 0.08	36.16	35.83	3.69	-19.48 ± 0.20	0.19	51.9	S	1e,4e
PGC 062709	33.80 ± 0.08	37.29	36.98	3.25	-22.41 ± 0.20	0.21	138.2	Sbc	1e,4e
IC 4820	32.99 ± 0.08	36.08	35.79	2.58	-19.12 ± 0.21	0.15	52.3	Sd	1e,4e
PGC 039904	32.04 ± 0.08	35.11	34.84	2.30	-16.72 ± 0.50	0.11	20.0	BCD	1e,4g
NGC 4204	31.97 ± 0.08	35.00	34.69	2.57	-17.70 ± 0.60	0.11	9.5	Sdm	1e,4h
PGC 039194	33.28 ± 0.08	36.83	36.44	2.82	21.52 ± 0.18	...	-20.59 ± 0.15	0.09	83.1	Sc	1e,2a,3g,4e
NGC 4158	32.59 ± 0.08	36.22	35.85	3.40	20.53 ± 0.25	...	-20.18 ± 0.40	0.11	32.8	Sb	1e,2a,3h,4e
A 1211+16	33.44 ± 0.08	36.71	36.47	1.70	21.71 ± 0.16	...	-21.11 ± 0.50	0.12	95.0	1e,2a,4e
PGC 038750	33.39 ± 0.08	21.78 ± 0.13	...	-20.24 ± 0.50	0.14	91.0	E	1e,2e,4e
NGC 4049	32.07 ± 0.08	35.29	35.00	2.72	-17.89 ± 0.50	0.08	20.0	I	1e,4g
NGC 4032	32.35 ± 0.08	35.63	35.35	2.47	20.50 ± 0.12	...	-19.37 ± 0.15	0.11	20.0	Im	1e,2a,4g
NGC 4455	32.09 ± 0.08	35.01	34.69	3.32	-18.09 ± 0.50	0.07	11.6	Sd	1e,4i
NGC 4635	32.42 ± 0.08	35.75	35.44	3.25	-19.47 ± 0.20	0.09	26.0	Sd	1e,3i,4d
NGC 4615	33.45 ± 0.08	36.90	36.60	2.89	21.71 ± 0.08	...	-20.74 ± 0.15	0.05	62.9	Scd	1e,2a,3g,4e
IC 3591	32.10 ± 0.08	35.28	35.05	1.60	-17.96 ± 0.50	0.08	21.8	Sm	1e,4i
NGC 4532	33.11 ± 0.08	36.82	36.62	1.74	22.03 ± 0.04	...	-20.31 ± 0.09	0.07	26.8	Im	1e,2a,4e
IC 3521	31.88 ± 0.08	35.74	35.48	2.23	20.24 ± 0.19	...	-18.38 ± 0.50	0.07	20.0	Sm	1e,2a,4g
IC 3414	32.05 ± 0.08	35.21	34.90	3.17	-18.17 ± 0.50	0.06	20.0	Sm	1e,4g
NGC 4423	32.06 ± 0.08	35.42	35.15	2.33	20.16 ± 0.22	...	-18.17 ± 0.50	0.07	20.0	Sm	1e,2a,4g
NGC 4430	32.32 ± 0.08	35.94	35.62	3.60	20.50 ± 0.12	...	-19.37 ± 0.50	0.06	20.0	Sb	1e,2a,4g
NGC 4470	32.48 ± 0.08	36.02	35.74	2.45	20.87 ± 0.07	...	-19.18 ± 0.50	0.08	20.0	Sa	1e,2a,4g
NGC 4376	32.22 ± 0.08	35.54	35.28	2.20	-18.38 ± 0.50	0.08	20.0	Im	1e,4g
IC 3322A	32.23 ± 0.08	36.29	35.97	3.16	20.98 ± 0.07	...	-19.07 ± 0.50	0.08	25.0	Im	1e,2a,4d+4i
IC 3268	32.26 ± 0.08	35.59	35.32	2.40	20.33 ± 0.17	...	-18.09 ± 0.50	0.08	20.0	Sm	1e,2a,4g
PGC 040993	32.41 ± 0.08	35.53	35.26	2.18	20.44 ± 0.20	...	-18.64 ± 0.50	0.07	26.0	Sbc	1e,2a,4i
NGC 4451	32.36 ± 0.08	36.43	36.14	2.71	20.89 ± 0.12	...	-20.11 ± 0.13	0.06	32.0	Sbc	1e,2a,4i
NGC 4276	32.52 ± 0.08	36.04	35.72	3.45	-20.01 ± 0.50	0.09	34.9	Sc	1e,4e
IC 3107	33.30 ± 0.08	36.97	36.68	2.80	21.86 ± 0.12	...	-21.47 ± 0.50	0.13	97.2	Sbc	1e,2a,4e
NGC 4383	32.62 ± 0.08	36.53	36.32	1.51	21.25 ± 0.05	...	-19.46 ± 0.10	0.08	20.0	Sa	1e,2a,4g
IC 0800	32.15 ± 0.08	35.40	35.10	2.93	-18.13 ± 0.50	0.12	20.0	Sc	1e,4g
NGC 4523	32.59 ± 0.08	35.46	35.14	3.41	20.14 ± 0.23	...	-17.52 ± 0.16	0.13	20.0	Sm	1e,2a,4g
NGC 4396	32.35 ± 0.08	35.94	35.62	3.39	20.99 ± 0.06	...	-19.01 ± 0.12	0.09	20.0	Sd	1e,2a,4g
IC 0797	32.18 ± 0.08	35.69	35.40	2.93	20.83 ± 0.07	...	-18.61 ± 0.50	0.10	20.0	Sc	1e,2f,4g
IC 3476	32.43 ± 0.08	35.88	35.61	2.40	20.56 ± 0.11	...	-18.90 ± 0.15	0.12	20.0	Im	1e,2a,4g
NGC 4670	32.20 ± 0.08	35.60	35.38	1.70	20.36 ± 0.07	...	-17.72 ± 0.15	0.05	11.8	S0	1e,2a,4j
NGC 6744	32.80 ± 0.08	36.32	35.96	3.86	-19.62 ± 0.20	0.14	6.5	Sbc	1e,3k,4k

TABLE A1—Continued

Galaxy Name	FUV ($\log_{10}[W/\text{\AA}^{-1}]$)	TIR ($\log_{10}[W]^{-1}$)	FIR _{Hetou} ($\log_{10}[W]^{-1}$)	100/60	1.4 GHz ($\log_{10}[W/\text{Hz}]^{-1}$)	f_{thermal}	V (mag)	A_V (mag)	D (Mpc)	H α ($\log_{10}[W]^{-1}$)	$A_{\text{H}\alpha, \text{Balmer}}$ (mag)	Type	References
NGC 4152	32.64 ± 0.08	36.33	36.07	2.12	21.19 ± 0.05	...	-19.40 ± 0.11	0.11	20.0	Sc	1e,2a,4g
NGC 4651	32.54 ± 0.08	36.55	36.27	2.71	21.21 ± 0.05	...	-20.77 ± 0.09	0.09	20.0	Sc	1e,2a,4g
NGC 4689	32.35 ± 0.08	36.37	36.03	4.31	20.78 ± 0.08	...	-20.63 ± 0.09	0.07	20.0	Sbc	1e,2a,4g
NGC 4535	32.95 ± 0.08	36.68	36.38	2.94	21.38 ± 0.04	...	-21.12 ± 0.09	0.06	16.0	Sc	1e,2a,4l
NGC 4519	32.77 ± 0.08	36.31	36.05	1.71	20.97 ± 0.06	...	-19.86 ± 0.07	0.07	21.0	Sd	1e,2a,4d
NGC 4522	32.01 ± 0.08	35.76	35.45	3.23	20.81 ± 0.05	...	-18.83 ± 0.40	0.07	15.6	Scd	1e,2a,4d
NGC 4567/8	32.51 ± 0.08	36.99	36.74	2.83	21.81 ± 0.04	...	-21.31 ± 0.30	0.11	20.0	Int	1e,2f,4g
NGC 4416	32.84 ± 0.08	36.46	36.13	2.90	21.01 ± 0.15	...	-20.80 ± 0.40	0.08	42.0	Scd	1e,2a,4i
NGC 4411B	32.79 ± 0.08	35.88	35.52	4.45	-20.01 ± 0.11	0.10	28.0	Scd	1e,4i
NGC 4424	31.90 ± 0.08	36.17	35.94	1.79	20.27 ± 0.18	...	-19.91 ± 0.09	0.07	20.0	Sa	1e,2a,4g
NGC 4380	32.09 ± 0.08	35.84	35.46	4.95	-19.91 ± 0.10	0.08	20.0	Sb	1e,4g
NGC 4438	32.30 ± 0.08	36.31	36.10	2.75	21.48 ± 0.04	...	-21.43 ± 0.07	0.09	20.0	S0	1e,2a,4g
NGC 4413	32.37 ± 0.08	35.85	35.55	3.07	-19.36 ± 0.16	0.10	20.0	Sab	1e,4g
NGC 4351	32.16 ± 0.08	35.66	35.37	2.85	-18.97 ± 0.15	0.10	20.0	Sab	1e,4g
NGC 4299	32.56 ± 0.08	20.92 ± 0.06	...	-19.13 ± 0.13	0.11	20.0	Sdm	1e,2a,4g
NGC 4178	32.62 ± 0.08	36.21	35.91	3.83	21.16 ± 0.05	...	-20.19 ± 0.09	0.09	20.0	Sdm	1e,2a,4g
NGC 4498	32.49 ± 0.08	35.95	35.64	3.25	20.28 ± 0.18	...	-19.40 ± 0.40	0.10	20.0	Sd	1e,2a,4g
NGC 4595	32.32 ± 0.08	35.82	35.50	3.09	20.35 ± 0.16	...	-19.33 ± 0.40	0.12	20.0	Sb	1e,2a,4g
NGC 4654	32.91 ± 0.08	36.93	36.65	2.67	21.77 ± 0.04	0.210 ± 0.062	-21.09 ± 0.10	0.08	20.0	34.15	0.61	Scd	1e,2a,4g,5c
NGC 4298	32.39 ± 0.08	36.77	36.42	3.85	-20.28 ± 0.09	0.12	20.0	Sc	1e,4g
NGC 4254	33.14 ± 0.08	37.34	37.04	2.67	22.31 ± 0.04	0.065 ± 0.039	-21.76 ± 0.08	0.13	20.0	34.73	0.84	Sc	1e,2a,4g,5c+5d
NGC 0450	...	36.12	35.88	2.05	20.80 ± 0.08	...	-18.97 ± 0.30	0.13	21.3	BCD	2a,3l,4m
NGC 1741	...	37.15	36.94	1.49	22.13 ± 0.05	...	-21.45 ± 0.50	0.17	59.8	BCD	2g,4m
NGC 2366	...	34.76	34.50	1.33	19.56 ± 0.06	...	-17.23 ± 0.12	0.12	3.9	BCD	2a,4m
MRK 0162	...	37.07	36.84	1.23	22.25 ± 0.06	...	-20.66 ± 0.50	0.03	96.6	BCD	2g,4m
UM 448	...	37.37	37.15	1.04	22.38 ± 0.05	...	-20.36 ± 0.50	0.08	78.5	BCD	2a,4m
UGC 06850	...	35.37	35.17	0.95	20.31 ± 0.13	...	-17.24 ± 0.50	0.06	17.2	BCD	2a,4m
NGC 4861	33.11 ± 0.12	36.11	35.86	1.25	20.97 ± 0.08	...	-19.72 ± 0.31	0.03	25.2	BCD	2a,4m
SBS 1533+574	...	35.89	35.66	1.58	21.16 ± 0.17	...	-17.97 ± 0.60	0.04	53.2	BCD	2g,3m,4m
NGC 2146	32.32 ± 0.11	37.45	37.22	1.41	22.43 ± 0.04	0.148 ± 0.040	-20.53 ± 0.13	0.31	14.5	34.05	...	Sab	1f,1b ² a
NGC 2595	33.41 ± 0.07	36.74	36.43	3.29	21.65 ± 0.08	...	-21.67 ± 0.14	0.13	57.7	Sc	1f,2a,4e
NGC 2976	31.55 ± 0.12	35.32	35.05	2.72	19.83 ± 0.04	...	-17.67 ± 0.13	0.23	3.3	Sc	1f,2a,4e
NGC 3027	32.53 ± 0.12	35.47	35.20	3.02	-19.10 ± 0.16	0.11	14.1	Sd	1f,4e
NGC 3077	31.64 ± 0.08	35.43	35.20	1.83	19.75 ± 0.05	...	-18.38 ± 0.13	0.22	4.0	I	1f,2a,4n
NGC 3206	32.35 ± 0.12	35.44	35.17	2.30	-18.98 ± 0.50	0.05	15.4	Scd	1f,4e
A 1029+54	32.38 ± 0.12	36.29	36.03	1.14	20.91 ± 0.06	...	-18.77 ± 0.50	0.04	20.2	Im	1f,2a,4o
NGC 3440	32.23 ± 0.12	35.67	35.40	2.29	20.71 ± 0.12	...	-18.66 ± 0.50	0.04	25.4	Sb	1f,2a,4e
NGC 3445	33.02 ± 0.12	36.26	36.05	2.03	21.33 ± 0.05	...	-19.68 ± 0.20	0.02	27.6	Sm	1f,2a,4e
NGC 3448	32.54 ± 0.18	36.35	36.13	1.88	21.30 ± 0.04	...	-19.26 ± 0.13	0.04	18.0	I	1f,2a,4e
NGC 3488	32.70 ± 0.13	36.24	35.90	3.75	-20.05 ± 0.50	0.04	39.9	Sc	1f,4e
NGC 3556	32.27 ± 0.05	36.60	36.33	2.51	21.47 ± 0.04	0.085 ± 0.049	-19.87 ± 0.10	0.06	9.3	33.70	...	Scd	1f,2a,4e,5d
NGC 3623	32.13 ± 0.20	36.18	35.80	5.11	20.30 ± 0.09	...	-21.40 ± 0.05	0.08	13.5	Sa	1f,2a,4p
NGC 3646	33.66 ± 0.12	22.43 ± 0.04	...	-22.71 ± 0.13	0.08	56.6	Sbc	1f,2a,4e
NGC 3726	33.05 ± 0.12	36.69	36.36	3.40	21.14 ± 0.05	0.085 ± 0.049	-21.14 ± 0.09	0.05	20.0	34.24	...	Sc	1f,2a,4h,5e
NGC 3782	32.05 ± 0.12	35.20	34.90	2.85	20.05 ± 0.09	...	-17.53 ± 0.50	0.06	9.9	Scd	1f,2a,4e
A 1137+46	32.01 ± 0.12	34.79	34.51	2.50	-17.76 ± 0.50	0.09	11.3	Sm	1f,4e
NGC 3811	32.83 ± 0.12	36.73	36.48	2.30	21.44 ± 0.07	...	-20.86 ± 0.40	0.06	41.4	Scd	1f,2a,4e
NGC 3877	32.33 ± 0.12	36.73	36.41	3.00	21.29 ± 0.05	...	-20.59 ± 0.10	0.08	20.0	Sc	1f,2a,4h
NGC 3888	32.75 ± 0.06	36.82	36.56	2.52	21.58 ± 0.05	...	-20.45 ± 0.15	0.04	32.1	Sc	1f,2a,4e
NGC 3893	33.14 ± 0.12	36.96	36.68	2.61	21.83 ± 0.04	...	-21.07 ± 0.50	0.07	20.0	Sc	1f,2a,4h
NGC 3906	32.26 ± 0.12	35.52	35.22	3.01	-18.59 ± 0.50	0.08	20.0	Sd	1f,4h
NGC 3913	32.26 ± 0.12	35.49	35.20	2.90	-18.95 ± 0.11	0.04	20.0	Sd	1f,4h
NGC 3928	32.07 ± 0.06	36.13	35.87	1.81	20.77 ± 0.08	...	-19.02 ± 0.13	0.06	20.0	Sb	1f,2a,4h
NGC 3938	33.18 ± 0.12	36.80	36.49	2.99	21.49 ± 0.04	...	-21.19 ± 0.10	0.07	20.0	Sc	1f,2a,4h
NGC 3949	32.99 ± 0.12	36.79	36.53	2.33	21.75 ± 0.04	...	-20.49 ± 0.15	0.07	20.0	Sbc	1f,2a,4h
NGC 3953	32.70 ± 0.12	36.85	36.48	4.44	21.33 ± 0.05	...	-21.53 ± 0.10	0.10	20.0	Sbc	1f,2a,4h
NGC 3972	32.22 ± 0.12	35.93	35.58	3.61	20.48 ± 0.12	...	-19.23 ± 0.16	0.05	20.0	Sbc	1f,2a,4h
NGC 3985	32.34 ± 0.12	35.91	35.63	2.41	20.84 ± 0.07	...	-18.99 ± 0.50	0.09	20.0	Sm	1f,2a,4h
A 1154+49	32.55 ± 0.12	35.74	35.40	3.79	-19.50 ± 0.50	0.10	20.0	Sd	1f,4h
NGC 4010	32.03 ± 0.12	36.16	35.83	4.03	20.99 ± 0.06	...	-19.08 ± 0.50	0.08	20.0	Sd	1f,2a,4h

TABLE A1—Continued

Galaxy Name	FUV ($\log_{10}[W/\text{\AA}]^{-1}$)	TIR ($\log_{10}[W]^{-1}$)	FIR _{Hellou} ($\log_{10}[W]^{-1}$)	100/60	1.4 GHz ($\log_{10}[W/\text{Hz}]^{-1}$)	f_{thermal}	V (mag)	A_V (mag)	D (Mpc)	H α ($\log_{10}[W]^{-1}$)	$A_{\text{H}\alpha, \text{Balmer}}$ (mag)	Type	References
A 1156+52	32.54 ± 0.12	35.47	35.10	4.59	-18.69 ± 0.50	0.09	20.0	Scd	1f,4h
NGC 4068	31.55 ± 0.12	34.09	33.77	3.66	-16.25 ± 0.50	0.07	5.2	Im	1f,4q
NGC 4189	33.24 ± 0.12	36.90	36.61	2.93	21.53 ± 0.06	...	-21.38 ± 0.08	0.11	40.0	Scd	1f,2a,4p
NGC 4190	30.96 ± 0.12	33.92	33.60	3.30	18.89 ± 0.14	...	-14.50 ± 0.31	0.10	3.5	Im	1f,2a,4r
IC 3061	32.93 ± 0.12	36.28	35.95	3.61	-19.90 ± 0.09	0.12	47.0	Sc	1f,4p
A 1212+36B	31.86 ± 0.12	34.77	34.55	1.54	-17.05 ± 0.50	0.05	12.6	Sdm	1f,4e
NGC 4212	32.76 ± 0.12	36.78	36.47	2.61	21.27 ± 0.05	...	-20.87 ± 0.08	0.11	24.2	Sc	1f,2a,4p
NGC 4217	32.00 ± 0.12	36.82	36.55	3.98	21.76 ± 0.04	...	-20.39 ± 0.10	0.06	20.0	Sb	1f,2a,4h
NGC 4234	32.39 ± 0.12	35.99	35.69	2.66	20.37 ± 0.15	...	-18.87 ± 0.20	0.06	20.0	Sm	1f,2a,4h
NGC 4237	32.72 ± 0.12	36.71	36.40	3.32	20.87 ± 0.13	...	-20.98 ± 0.11	0.10	32.0	Sbc	1f,2a,4p
NGC 4274	32.12 ± 0.12	36.50	36.23	3.05	20.75 ± 0.09	...	-21.32 ± 0.13	0.07	21.4	Sab	1f,2a,4p
NGC 4275	32.55 ± 0.12	36.34	36.03	2.32	20.92 ± 0.11	...	-19.01 ± 0.50	0.07	30.8	S	1f,2a,4e
NGC 4273	33.15 ± 0.12	37.30	37.03	2.00	22.14 ± 0.04	...	-21.11 ± 0.09	0.06	38.2	Sc	1f,2a,4p
NGC 4303A	32.19 ± 0.12	35.20	34.95	1.89	-18.04 ± 0.09	0.08	15.5	Scd	1f,4d
NGC 4314	32.44 ± 0.21	35.84	35.63	1.88	20.41 ± 0.07	...	-20.05 ± 0.15	0.08	12.8	Sa	1f,2a,4e
IC 3255	33.31 ± 0.06	36.71	36.46	2.10	-19.76 ± 1.00	0.08	86.4	Sbc	1f,4e
IC 3258	31.64 ± 0.06	35.38	35.13	1.96	-18.52 ± 0.13	0.11	20.0	Im	1f,4h
NGC 4369	32.19 ± 0.12	36.12	35.89	1.96	20.74 ± 0.05	...	-19.13 ± 0.13	0.08	13.9	Sa	1f,2a,4e
NGC 4390	32.03 ± 0.06	35.64	35.36	2.52	-18.91 ± 0.50	0.10	20.0	Sbc	1f,4h
NGC 4393	32.02 ± 0.12	34.89	34.54	4.25	19.98 ± 0.10	...	-18.00 ± 0.50	0.09	10.1	Sd	1f,2e,4s
NGC 4402	32.19 ± 0.06	36.81	36.47	3.22	21.30 ± 0.05	...	-19.98 ± 0.50	0.09	25.0	Sb	1f,2a,4p+4d
NGC 4412	32.39 ± 0.12	36.18	35.91	1.87	20.85 ± 0.07	...	-18.96 ± 0.50	0.06	20.0	Sb	1f,2a,4h
NGC 4420	32.34 ± 0.12	35.92	35.68	2.47	-18.64 ± 0.50	0.06	15.0	Sbc	1f,4t
NGC 4457	31.65 ± 0.12	35.85	35.61	1.97	20.56 ± 0.05	...	-19.37 ± 0.16	0.07	11.0	S0	1f,2a,4t
NGC 4480	32.76 ± 0.12	36.38	36.06	3.48	20.61 ± 0.23	...	-20.30 ± 0.11	0.08	34.0	Sc	1f,2a,4t
NGC 4490	32.80 ± 0.06	36.51	36.31	1.80	21.81 ± 0.04	0.049 ± 0.025	-19.80 ± 0.06	0.07	8.0	34.28	...	Sd	1f,2h,4u,5f
NGC 4525	31.98 ± 0.06	35.55	35.17	5.28	-19.28 ± 0.50	0.07	20.0	Scd	1f,4h
NGC 4568	32.87 ± 0.06	37.34	37.05	2.79	22.03 ± 0.04	...	-21.37 ± 0.09	0.11	26.0	Sbc	1f,2a,4p
NGC 4605	32.05 ± 0.04	35.70	35.46	2.29	20.43 ± 0.04	...	-18.30 ± 0.09	0.05	5.2	Sc	1f,2a,4v
NGC 4618	32.20 ± 0.12	35.48	35.22	2.65	20.26 ± 0.05	...	-18.35 ± 0.04	0.07	6.5	Sm	1f,2a,4d
NGC 4625	31.39 ± 0.12	35.03	34.72	2.97	19.65 ± 0.11	...	-17.00 ± 0.04	0.06	7.2	Sm	1f,2a,4d
NGC 4632	32.30 ± 0.12	36.06	35.80	2.90	20.94 ± 0.05	...	-19.01 ± 0.50	0.08	14.0	Sc	1f,2a,4d
NGC 4634	32.08 ± 0.12	36.38	36.12	2.83	21.20 ± 0.05	...	-19.21 ± 0.09	0.09	20.0	Scd	1f,2a,4h+4i
NGC 4642	32.58 ± 0.12	36.21	35.90	3.08	21.11 ± 0.10	...	-19.66 ± 0.50	0.08	36.0	Sbc	1f,2a,4p
NGC 4653	33.01 ± 0.12	36.26	35.94	3.44	-20.57 ± 0.09	0.08	35.0	Scd	1f,4e
NGC 4666	32.61 ± 0.12	37.30	37.04	2.22	22.32 ± 0.04	...	-20.85 ± 0.10	0.08	20.0	Sc	1f,2a,4d
NGC 4688	32.23 ± 0.12	35.33	35.07	2.13	-18.69 ± 0.50	0.10	13.1	Scd	1f,4e
NGC 4691	32.74 ± 0.12	36.91	36.63	1.50	-20.72 ± 0.13	0.09	22.0	S0	1f,4w
NGC 4701	33.19 ± 0.12	36.66	36.39	2.35	21.44 ± 0.06	...	-20.44 ± 0.10	0.10	35.0	Scd	1f,2a,4p
NGC 4713	32.41 ± 0.12	35.76	35.55	2.39	20.39 ± 0.06	...	-18.48 ± 0.11	0.09	10.5	Sd	1f,2a,4d
NGC 4747	32.07 ± 0.12	35.67	35.40	2.47	20.18 ± 0.11	...	-18.25 ± 0.13	0.03	13.0	Scd	1f,2a,4d
NGC 4765	31.79 ± 0.12	35.39	35.14	1.94	20.30 ± 0.06	...	-17.05 ± 0.10	0.13	9.7	S0	1f,2a,4e
NGC 4779	32.92 ± 0.12	36.55	36.28	2.12	21.15 ± 0.10	...	-20.36 ± 0.50	0.07	37.7	Sbc	1f,2a,4e
NGC 4808	32.61 ± 0.12	36.58	36.30	2.23	21.46 ± 0.04	...	-19.89 ± 0.10	0.12	20.0	Scd	1f,2a,4h
NGC 4868	33.90 ± 0.12	37.27	37.00	2.64	22.09 ± 0.05	...	-21.62 ± 0.50	0.05	62.2	Sab	1f,2a,4e
NGC 4900	32.84 ± 0.12	36.53	36.25	2.26	21.35 ± 0.04	...	-20.21 ± 0.17	0.08	20.0	Sc	1f,2a,4j
NGC 4961	32.44 ± 0.12	36.27	35.99	2.74	21.09 ± 0.10	...	-19.13 ± 0.23	0.04	33.8	Scd	1f,2a,4e
A 1307+34	31.68 ± 0.12	34.56	34.28	2.53	-16.21 ± 0.50	0.03	10.8	Scd	1f,4e
NGC 5012	33.09 ± 0.12	36.72	36.43	2.93	21.64 ± 0.05	...	-20.76 ± 0.50	0.05	34.9	Sc	1f,2a,4e
NGC 5016	32.59 ± 0.12	36.43	36.11	3.01	20.87 ± 0.15	...	-19.85 ± 0.50	0.04	34.8	Sc	1f,2a,4e
A 1310+36	32.19 ± 0.12	35.03	34.72	3.16	-17.43 ± 0.16	0.06	12.6	Im	1f,4e
A 1312+35	31.71 ± 0.12	34.85	34.61	1.73	-16.60 ± 0.31	0.05	11.5	Im	1f,4e
NGC 5195	33.12 ± 0.12	36.07	35.79	1.87	20.87 ± 0.04	...	-19.97 ± 0.07	0.12	7.6	S0	1f,2a,4x
NGC 5320	33.07 ± 0.12	36.38	36.06	3.45	20.97 ± 0.12	...	-20.54 ± 0.50	0.02	34.9	Sc	1f,2a,4e
NGC 5350	33.25 ± 0.12	36.63	36.32	3.95	21.29 ± 0.06	...	-21.15 ± 0.12	0.04	30.9	Sb	1f,2a,4e
NGC 5368	32.97 ± 0.12	36.80	36.55	2.23	21.62 ± 0.09	...	-20.70 ± 0.50	0.04	61.9	Sab	1f,2a,4e
NGC 5371	33.41 ± 0.12	37.11	36.75	3.36	21.93 ± 0.04	...	-22.07 ± 0.14	0.03	34.0	Sbc	1f,2a,4e
NGC 5383	32.67 ± 0.09	36.82	36.55	2.52	21.50 ± 0.05	0.151 ± 0.101	-21.01 ± 0.04	0.02	30.0	34.68	...	Sb	1f,2a,4e,5g
NGC 5474	32.27 ± 0.05	35.06	34.76	3.61	19.82 ± 0.08	...	-18.41 ± 0.16	0.03	6.8	Scd	1f,2a,4e
NGC 5477	31.31 ± 0.12	34.29	34.05	1.76	-15.46 ± 0.15	0.04	7.7	Sm	1f,4v

TABLE A1—Continued

Galaxy Name	FUV ($\log_{10}[W/\text{\AA}]^{-1}$)	TIR ($\log_{10}[W]^{-1}$)	FIR _{Helou} ($\log_{10}[W]^{-1}$)	100/60	1.4 GHz ($\log_{10}[W/\text{Hz}]^{-1}$)	f_{thermal}	V (mag)	A_V (mag)	D (Mpc)	H α ($\log_{10}[W]^{-1}$)	$A_{\text{H}\alpha, \text{Balmer}}$ (mag)	Type	References
NGC 5486	32.18 ± 0.12	35.37	35.10	2.29	-18.20 ± 0.50	0.06	18.5	Sm	1f,4e
NGC 5806	32.15 ± 0.12	36.15	35.87	2.93	20.78 ± 0.07	...	-19.76 ± 0.22	0.17	18.1	Sb	1f,2a,4e
NGC 5874	32.50 ± 0.12	36.25	35.91	3.95	-20.72 ± 0.17	0.07	41.7	Sc	1f,4e
NGC 5879	32.02 ± 0.12	35.82	35.54	3.04	20.50 ± 0.06	...	-18.78 ± 0.10	0.04	11.6	Sbc	1f,2a,4y
NGC 5907	32.71 ± 0.07	36.69	36.31	5.21	21.39 ± 0.04	0.208 ± 0.052	-20.43 ± 0.11	0.03	14.0	33.78	...	Sc	1f,2a,4z,5d
NGC 6207	32.24 ± 0.12	35.89	35.65	2.74	20.74 ± 0.05	...	-18.70 ± 0.10	0.05	11.4	Sc	1f,2a,4y
NGC 6503	31.63 ± 0.04	35.33	35.03	2.85	19.76 ± 0.05	...	-17.66 ± 0.09	0.10	3.6	Scd	1f,2a,4y
NGC 7625	32.15 ± 0.04	36.71	36.45	2.01	21.54 ± 0.04	...	-19.68 ± 0.13	0.08	21.8	Sa	1f,2a,4e
NGC 7677	33.07 ± 0.12	37.00	36.74	1.50	21.66 ± 0.06	...	-20.33 ± 0.13	0.14	47.4	Sbc	1f,2a,4e

References. — *UV data*: (1a) Bell (2002); (1b) Bell & Kennicutt (2001); (1c) Measured directly from the IUE spectra; (1d) Goldader et al. (2002); (1e) Deharveng et al. (1994); (1f) Rifatto, Longo & Capaccioli (1995b) — *Radio data*: (2a) Condon et al. (2002); (2b) Condon et al. (1998); (2c) Becker, White & Helfand (1995); (2d) Wright et al. (1994); (2e) Gavazzi & Boselli (1999b); (2f) Gavazzi & Boselli (1999a); (2g) Hopkins et al. (2002); (2h) White & Becker (1992) — *Optical V-band data*: (3a) Calzetti et al. (1995) assuming $B-V = 0.4$; (3b) Maddox et al. (1990) assuming $B-V = 0.5$; (3c) Spingoglio et al. (1995) assuming $B-K = 4.5$ (the average for the other ULIRGs); (3d) de Vaucouleurs et al. (1991) assuming $B-V = 0.5$; (3e) Han (1992); (3f) Lauberts & Valentijn (1989), by averaging B and R ; (3g) Gavazzi & Boselli (1996); (3h) Gavazzi & Boselli (1996)+de Vaucouleurs et al. (1991); (3i) de Vaucouleurs et al. (1991)+Takamiya, Kron & Kron (1995); (3k) de Vaucouleurs & Longo (1988); (3l) Mathewson & Ford (1996) converted from I -band; (3m) Doublier et al. (1997) — *Distances*: (4a) Lee et al. (2002); (4b) Calzetti et al. (1994); (4c) Goldader et al. (2002); (4d) Teerikorpi et al. (1992); (4e) Hubble flow, assuming $H_0 = 75 \text{ km s}^{-1} \text{ Mpc}^{-1}$; (4f) Karachentsev (2002); (4g) Virgo Cluster and Ursa Major Cluster distances following Shanks (1997) and Sakai et al. (2000); (4h) Jansen et al. (2000); (4i) Yasuda, Fukugita & Okamura (1997); (4j) Tully & Shaya (1984); (4k) Bottinelli et al. (1984); (4l) Macri et al. (1999); (4m) Hopkins et al. (2002); (4n) Tonry et al. (2001); (4o) Mas-Hesse & Kunth (1999); (4p) Ekholm et al. (2000); (4q) Makarova, Karachentsev & Georgiev (1997); (4r) Tikhonov & Karachentsev (1998); (4s) From membership in the Coma 1 cloud at 10 Mpc; (4t) Gavazzi et al. (1999); (4u) Clemens, Alexander & Green (1999); (4v) Karachentsev & Makarova (1996); (4w) Garcia-Barreto et al. (1995); (4x) Bell & Kennicutt (2001); (4y) Bottinelli et al. (1986); (4z) Zepf et al. (2000) — *H α data*: (5a) Calzetti et al. (1995); (5b) Wu et al. (1998); (5c) Kennicutt & Kent (1983); (5d) Young et al. (1996); (5e) Romanishin (1990); (5f) Kennicutt et al. (1987); (5g) Sheth et al. (2000)

^aBell & Kennicutt (2001) presents all of the data except for the radio luminosity.

^bThis galaxy has a major axis optical diameter $\geq 1.5'$, so its UV data is ignored to minimize aperture bias.

^cBell & Kennicutt (2001) presents all of the data for this galaxy except for the UV flux and radio luminosity: the UV flux is taken from Rifatto, Longo & Capaccioli (1995b).

^dThe radio data are also taken from Bell & Kennicutt (2001) for NGC 4038/9 and NGC 253.

Note. — The IR data are taken from (in order of preference) Rice et al. (1988), Soifer et al. (1989), and Moshir et al. (1990). The optical data are taken from the RC3 (de Vaucouleurs et al. 1991) or the ESO-LV catalog (Lauberts & Valentijn 1989) unless otherwise stated. Thermal radio fractions are taken from (in order of preference) Bell & Kennicutt (2001) and Niklas et al. (1997). Note that Bell & Kennicutt (2001) obtains thermal fractions from a variety of sources, with the majority from Niklas et al. (1997). Balmer decrements are taken from Bell & Kennicutt (2001) for normal galaxies (and are averages of individual H II region Balmer decrements) and from Calzetti et al. (1994) and Wu et al. (1998) for starbursting galaxies and ULIRGs respectively.